Tectonics®

RESEARCH ARTICLE
10.1029/2025TC008815

Active Crustal Deformation Across a Nucleating Extensional Microplate, D. R. Congo, East Africa

Meritxell Colet[1], Folarin Kolawole[1], Rasheed Ajala[2], Damien Delvaux[3], and Hardy Medry Dieu-Veill Nkodia[4]

[1]Department of Earth and Environmental Sciences, Columbia University, New York, NY, USA, [2]Lamont-Doherty Earth Observatory, Columbia University, New York, NY, USA, [3]Department of Geology, Royal Museum for Central Africa, Tervuren, Belgium, [4]Marien Ngouabi University, Brazzaville, Republic of Congo

Key Points:

- The Luama and Kamituga Rifts in D.R. Congo host prominent seismicity and widespread active fault scarps deforming the Holocene surface
- The faults exhibit high slip tendencies in the East African Rift stress field, link to Kivu and Tanganyika rifts, and define a microplate
- Diffuse seismicity across the microplate indicates active penetrative deformation or that microplate nucleation is in an incipient phase

Supporting Information:

Supporting Information may be found in the online version of this article.

Correspondence to:

M. Colet,
mcolet@ldeo.columbia.edu

Citation:

Colet, M., Kolawole, F., Ajala, R., Delvaux, D., & Dieu-Veill Nkodia, H. M. (2025). Active crustal deformation across a nucleating extensional microplate, D. R. Congo, East Africa. *Tectonics*, *44*, e2025TC008815. https://doi.org/10.1029/2025TC008815

Received 12 JAN 2025
Accepted 19 JUN 2025

Author Contributions:

Conceptualization: Meritxell Colet, Folarin Kolawole
Data curation: Folarin Kolawole
Formal analysis: Meritxell Colet, Folarin Kolawole
Funding acquisition: Folarin Kolawole
Investigation: Meritxell Colet, Folarin Kolawole, Damien Delvaux
Methodology: Meritxell Colet, Folarin Kolawole
Project administration: Folarin Kolawole
Resources: Folarin Kolawole
Software: Folarin Kolawole, Rasheed Ajala
Supervision: Folarin Kolawole
Validation: Folarin Kolawole
Visualization: Meritxell Colet, Folarin Kolawole
Writing – original draft: Meritxell Colet, Folarin Kolawole

Abstract Active tectonic fragmentation of continents is commonly accommodated by continental-scale networks of rift basins and microplates along the evolving divergent plate boundaries. Yet, little is known about deformational processes that accompany the incipient stages of microplate development. We explore the East Africa's Western Rift, where the Nubian-Victoria plate boundary is collocated with a ∼200-km-wide region of seismicity, low-wave-speed lithosphere, and hot springs that continue outboard of the commonly proposed active rift axis and westward into the Congo Craton, across the polydeformed Precambrian orogenic belts. We investigate a network of two contiguous, poorly studied rift basins in eastern DRC: the NW-striking Luama Rift, commonly characterized as a "failed" Mesozoic rift, and its adjacent NE-striking Kamituga Rift, located cratonward. We perform fault mapping, earthquake-based stress inversion, reactivation tendency and fault attribute analyses to characterize the axes and mechanisms of active extension. In the two rift basins, we unveil and analyze previously unknown systems of 2–170-km long active faults with 10–130-m high scarps, and resolve their contemporary stress states and length-scale attributes. The results reveal: (a) failure-optimal orientation of faults in the contemporary EARS stress field, (b) fault-length scale distribution that manifests rejuvenation of the Luama Rift, and incipient rifting in the Kamituga Rift as a southwestward continuation of the Kivu Rift. The axes of extension delineate a previously unknown microplate, herein named the "Itombwe Microplate"; however, we propose that diffuse seismicity across the microplate indicates its non-rigidity or that microplate nucleation is still incipient.

Plain Language Summary The break-up of continents is manifested at the Earth's surface through the formation of rift basins and microplates. However, the deformation in the early stages of microplate development and evolution remain poorly understood. This study focuses on the Western Branch of the East African Rift System (EARS), where the boundary between the Nubian and Victoria plates overlaps with a ∼200 km-wide zone of seismicity, hot springs, and low seismic wave speeds that extend westward into the Congo Craton. We investigate two poorly studied rift basins in eastern Democratic Republic of Congo: the NW-striking Luama Rift, traditionally classified as a failed Mesozoic rift, and the adjacent NE-striking Kamituga Rift. Through detailed fault mapping, earthquake stress inversion, and analysis of fault scarp lengths, we identify previously undocumented active fault systems that indicate ongoing tectonic activity. We find that these faults are optimally oriented in the current EARS stress regime, suggesting that the previously considered inactive Luama and Kamituga Rifts are reactivating. Together, these rifts bound a newly recognized tectonic block, the Itombwe Microplate, which appears to be in an early stage of development.

1. Introduction

Divergent plate boundaries initiate as continental-scale networks of rift basins and commonly initiate microplates at adjacent rift branches or rift segments. Structures inherited from previous deformation episodes often facilitate and guide the development of geometry, orientation, and evolution of the tectonic boundary at different scales (e.g., Brune et al., 2023). At the scale of rift systems (>1,000s km), observations and numerical models suggest that rift location and architecture may be controlled by the presence of crustal-scale mechanical weaknesses such as suture zones and other fault systems found in orogenic belts ringing ancient cratons (e.g., Corti et al., 2007, 2022; Daly et al., 1989; Gouiza & Naliboff, 2021; Laó-Dávila et al., 2015; Withjack et al., 2012). At the scale of individual rift segments (>100s km), reactivation of inherited basement structures such as anisotropic rock fabrics or pre-existing faults from previous tectonic events, exert a strong influence over strain distribution and the

Writing – review & editing: Meritxell Colet, Folarin Kolawole, Rasheed Ajala, Damien Delvaux, Hardy Medry Dieu-Veill Nkodia

evolution and geometry of the overlying rift (Kolawole, Phillips, et al., 2021; Kolawole et al., 2022; Phillips et al., 2016). However, failed rifts might not necessarily reactivate along the inherited weaknesses if the mantle lithosphere has cooled and strengthened between rifting events, instead migrating adjacent to the original rift (Naliboff & Buiter, 2015). At the fault scale, normal faults localize within the mobile belts (Kibaran, Ubendian, Ruwenzori belts) at the craton edge (McConnell, 1967, 1972; Ring, 1994; Versfelt & Rosendahl, 1989). Favorably oriented inherited fabrics, faults, foliation, and shear zones facilitate and modulate fault geometry, strain accommodation, and seismicity (e.g., Corti et al., 2022; Kirkpatrick et al., 2013; Kolawole et al., 2018; Ratcliffe et al., 1986; Samsu et al., 2023; Wedmore et al., 2020). For continental microplates in extensional regimes, geodynamic studies suggest that the spatial distribution of inherited lithospheric weaknesses (e.g., mobile belts) exerts a first-order control on microplate kinematics, and offset rift segments can facilitate microplate formation (Glerum et al., 2020; Neuharth et al., 2021). Yet, little is known about active deformation at incipient microplates in natural settings.

Here, we examine first-order patterns of active deformation during the initiation of a continental divergent plate boundary and extensional microplate. We explore this problem in the Luama-Kamituga Rift Zone, located in the eastern Democratic Republic of Congo (DRC), which hosts basement terranes that has witnessed polyphase orogenesis of three structurally distinct orogenic belts: the Paleoproterozoic NW-trending Ruzizian-Ubendian Belt, the Mesoproterozoic NW-trending Kibaran Belt, and the heavily folded Karagwe-Ankole Belt. Located in the East African Rift System (EARS) (Figure 1a), the rift zone encompasses a network of two poorly studied rifts, the "failed" Luama Rift and the adjacent Kamituga Rift (Figures 1b and 1c). We integrate legacy geology maps, Digital Elevation Model (DEM) hillshade maps, rift morphology, reactivation tendency, and fault length scaling analytical techniques to characterize the Luama and Kamituga Rifts. We present results demonstrating the ongoing tectonic reactivation of the Luama Rift and progressive development of the Kamituga Rift, and provide insights into the sources of stress perturbation that drive faulting, seismicity, and rift evolution. We show how the inheritance of a polyphase orogenic lithosphere provides a template for microplate nucleation between the evolving rifts.

2. Geological Setting of the Luama-Kamituga Rift Zone

2.1. The Pre-Rift Crystalline Basement

The pre-rift crystalline basement of the Luama-Kamituga Rift Zone is composed of three main belts: the Paleoproterozoic NW-trending Ruzizian-Ubendian, the Mesoproterozoic NE-trending Kibaran and Karagwe-Ankole, and the Neoproterozoic Itombwe Belt. These belts evolved between the Archean Tanzania craton and the Archean-Paleoproterozoic Congo craton.

2.1.1. The Paleoproterozoic Ruzizian-Ubendian Belt

The Paleoproterozoic (2.1–1.8 Ga) Ruzizian-Ubendian Belt is a ca. 600 km-long and 150 km-wide transcurrent NW–SE striking orogenic belt with a consistent NW–SE striking fabric (Figure 1c). It comprises the most extensively studied Ubende Belt in Tanzania and its poorly studied continuation into the DRC (Ruzizian Belt), across Lake Tanganyika. The Ubende Belt consists of 2,100–2,025 Ma high-grade protolith, exhumed under amphibolite-facies conditions in the 1,950–1,850 Ma time interval; Paleo- and Neo-proterozoic eclogites, granitoid, and associated volcanic intrusions (Boniface et al., 2012; Boniface & Schenk, 2012; Boven et al., 1999; Lenoir et al., 1994; Theunissen et al., 1996). On its northern end, the Ubendian Belt is overlain by metasedimentary rocks of the Mesoproterozoic Karagwe-Ankole Belt and metamorphosed sedimentary rocks and lavas of the Neoproterozoic Malagarasi Platform (Deblond et al., 2001; Leger et al., 2015). Based on lithology and structural characteristics, the Ubendian Belt is composed of eight terranes (Ubende, Wakole, Katuma, Ufipa, Mbozi, Lupa, Upangwa, and Nyika Terranes), bounded by steeply dipping, mylonitic ductile dextral strike-slip shear zones (Boven et al., 1999; Daly, 1988; Theunissen et al., 1996). More recently, Boniface and Tsujimori (2021) proposed three groups based on similar geology and age distribution: the Eastern Ubendian Corridor (Katuma and Lupa Terranes), the Central Ubendian Corridor (Ubende, Mbozi, and Upangwa Terranes), and the Western Ubendian Corridor, excluding the Wakole Terrane.

Previous studies have interpreted the Ubendian Belt to have undergone two main phases of deformation (Daly, 1988). The adjacent Usagaran Belt initially developed as NW-directed thrust sheets that overthrust the Tanzanian Craton. Subsequently, the Ubendian terranes formed as a series of tectonic slivers that accreted along

10.1029/2025TC008815

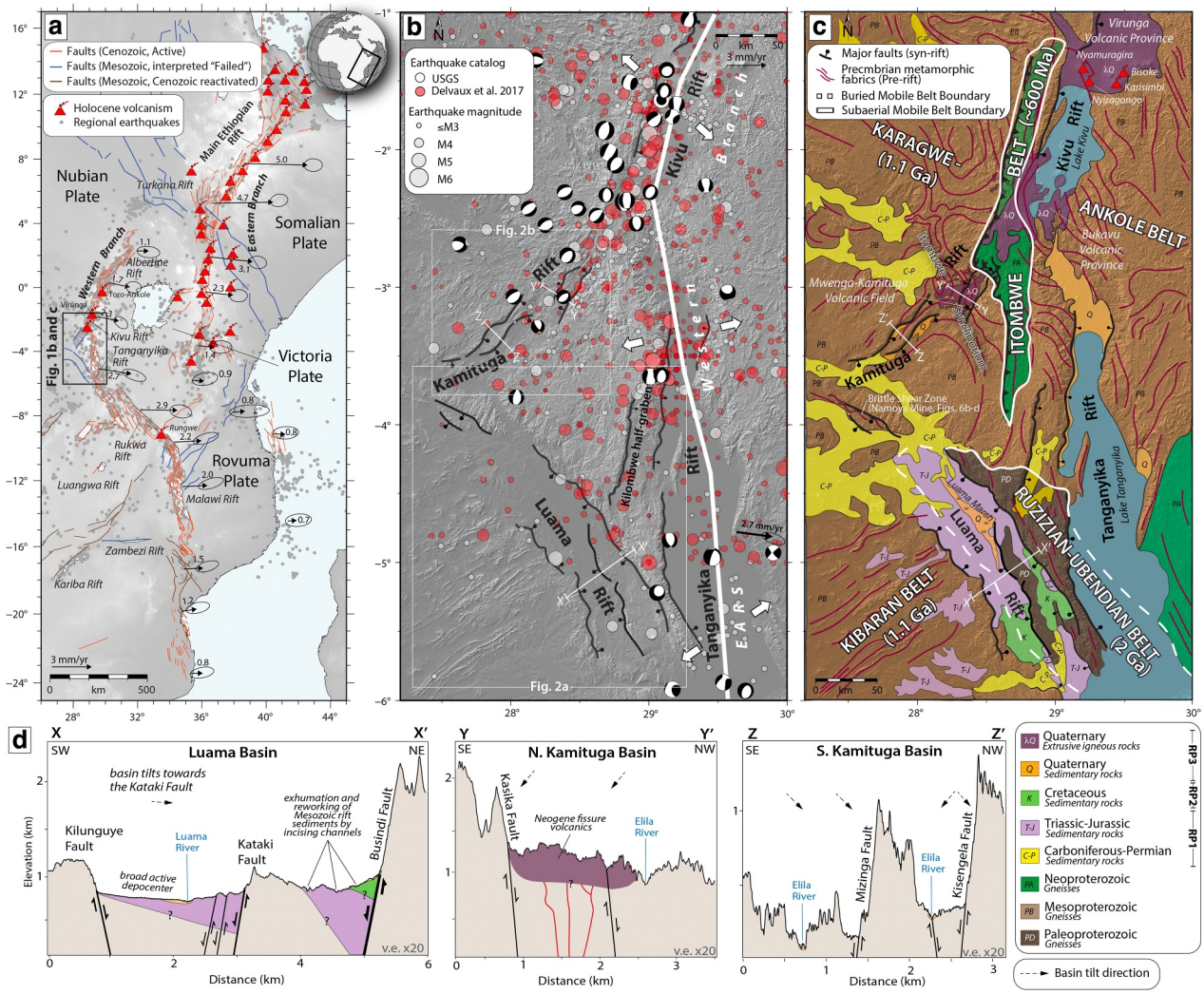

Figure 1. Map of the East African Rift System (EARS) and the Luama-Kamituga Rift Zone study area. (a) Overview map of the EARS showing Mesozoic and Cenozoic active, failed, and reactivated rift faults, Holocene volcanism, GPS vectors with 95% confidence error ellipses (Saria et al., 2014), and regional earthquakes (gray circles). The estimated average horizontal error of the USGS earthquake locations is 8 km with standard deviation of 2 km, and average vertical error of 3 km with standard deviation of 5 km. Map modified from Ajala et al. (2024). (b) Shuttle Radar Topography Mission (SRTM)-Digital Elevation Model hillshade map of the Luama-Kamituga Rift Zone showing earthquakes (white and red circles, USGS and Delvaux et al., 2017), moment tensors (Ekstrom et al., 2012), and the regional stress fields (white arrows, Delvaux & Barth, 2010). (c) Geological map of the Luama-Kamituga Rift Zone overlaid on a SRTM hillshade map (modified after Choubert and Faure-Muret (1987), Delvaux (1989), Kröner (1977), Laghmouch et al. (2018), Thiéblemont et al. (2018), Veatch and Geological Society of America (1935), and Villeneuve (1987)). In the legend, RP1 refers to "Rift Phase 1," corresponding to the Early Mesozoic phase of tectonic extension in East Africa, popularly known as the "Karoo rifting event." RP2 refers to "Rift Phase 2." It corresponds to the Late Jurassic-Early Cretaceous rifting event in East Africa, recorded in many Karoo rift basins, and marking a reactivation of the Karoo basins. RP3 refers to "Rift Phase 3," corresponding to another phase of tectonic extension which initiated in the Miocene-Oligocene. See Section 2.2 for more details. (d) Elevation along profiles X–X′, Y–Y′, and Z–Z′, highlighted by white lines in panels b and c, showing geologic features of the rifts.

the margin of the Tanzanian Craton. Other studies proposed that an early Paleoproterozoic oblique suture preceded the main lateral shear deformation of the Ubendian Belt (Theunissen et al., 1996). Recent studies have revisited the tectonic model of Daly (1988) to propose three discrete episodes of terrane formation and evolution in the Ubendian Belt related to oceanic subduction and collisions between Tanzania, Bangweulu, and Congo Cratons during the Proterozoic (Boniface et al., 2012; Boniface & Schenk, 2012; Boniface & Tsujimori, 2021; Ganbat et al., 2021).

The Ruzizian Belt (Cahen, 1952, 1954; Lavreau, 1985) separates the two segments of the Mesoproterozoic orogeny: the Kibaran Belt in Katanga (Kokonyangi et al., 2004, 2005), and the Karagwe-Ankole Belt in Rwanda, Burundi, Kivu, NW Tanzania and SW Uganda (Fernandez-Alonso et al., 2012).

2.1.2. The Mesoproterozoic Kibaran and Karagwe-Ankole Belts

The Mesoproterozoic (1.1 Ga) Kibaran and Karagwe-Ankole Belts trend NE–SW, extending from the Katanga region in the DRC to the Ankole region in SW Uganda. The outcrops of the Mesoproterozoic belts are surrounded by outcrops of the Paleoproterozoic Ruzizian-Ubendian Belt, associated with the unveiling of the Precambrian terranes and terrane boundaries by long-term erosion of the Mesoproterozoic cover rocks (Figure 1c). The Kibaran orogeny reworked the western Ruzizian-Ubendian terranes at the region of overlap (Luama Rift region, Figure 1c). At the Namoya Mine, DRC (Figure 1c; other gold mines along the Ubendian Belt described in Dunn & von der Heyden, 2022; Evans et al., 2012; Kazimoto et al., 2014), a large brittle shear zone hosting hydrothermal gold alterations in Mesoproterozoic rocks (De Bie, 2015), strikes parallel to the Ruzizian-Ubendian Belt fabric, suggesting that the reactivation of the inherited Paleoproterozoic fabrics was likely not intense in the region of the Luama Rift.

The Kibaran Belt consists predominantly of Paleo- and Meso-proterozoic sediments, covered by younger Neoproterozoic and Phanerozoic sedimentary rocks that have been intruded by different generations of granitoid rocks and minor associated mafic rocks. The belt has been interpreted as either having evolved during successive stages of subduction-driven accretionary and eventual collisional tectonics between ca. 1,400 and 1,000 Ma (Debruyne et al., 2015; Kampunzu et al., 1986; Kokonyangi et al., 2004, 2005, 2006), as an intracratonic orogenic chain with different consecutive periods of extension and compression (Klerkx et al., 1984, 1987), or marked by an intraplate tectonic-magmatic event at ca. 1,375 Ma in an extensional context (Fernandez-Alonso et al., 2012; Tack et al., 2010).

The Karagwe-Ankole Belt has two structurally contrasting domains, the Western Domain and the Eastern Domain, separated by the Kabanga-Musongati alignment, which is composed of mafic and ultramafic layered igneous complexes (Tack et al., 1994). The Western Domain is characterized by greenschist-to-amphibolite-facies Mesoproterozoic metasedimentary rocks and granitoid rocks, and the Eastern Domain is characterized by basal conglomerate and metasediment (e.g., Fernandez-Alonso et al., 2012; Tack et al., 1994). Recent studies have discovered Neoarchean crust exposed in the Paleoproterozoic Ruzizian-Ubendian terranes of the Western Dominion, interpreted as representing a reworked NW margin of the stable nucleus of the Tanzania Craton (Nambaje et al., 2020). Some studies have interpreted the Karagwe-Ankole Belt to have developed under intraplate conditions within the already consolidated Archean-Paleoproterozoic Craton in ca. 1,375 Ma (Fernandez-Alonso et al., 2012; Tack et al., 2010), while other studies have suggested a convergent setting along an active continental margin (e.g., Kampunzu et al., 1986; Nambaje et al., 2020; Rumvegeri, 1991).

2.1.3. The Neoproterozoic Itombwe Belt

The Neoproterozoic (1,020–575 Ma) Itombwe Belt is a >300 km-long and >50 km-wide fold-thrust belt located between Lake Kivu and Kamituga Rift (Cahen et al., 1979; Villeneuve, 1977). This elongated folded structure, which hosts the Itombwe Synclinorium, is composed of metasedimentary rocks metamorphosed to greenschist facies, diamictites of possible glacial origin, and granitoids (Gloire et al., 2022; Ilombe et al., 2017). The Itombwe Belt has undergone two major deformation phases (Gloire et al., 2022; Ilombe et al., 2017; Walemba, 2001). First, a phase of E–W axis folding during the Mesoproterozoic, and a second phase in an N–S synclinorium (Itombwe Synclinorium, Figure 1c), representing the effect of the Pan-African amalgamation of the Gondwana continent (Ilombe et al., 2017; Villeneuve, 1977, 1987), and perhaps kinematically linked with the strike-slip reactivation of the Ubendian Belt during the Pan-African orogenesis (Fernandez-Alonso & Theunissen, 1998; Theunissen et al., 1992).

2.2. Phanerozoic in East Africa

The EARS delineates the plate boundaries between the Nubian and Somalian plates and the Victoria and Rovuma microplates in East Africa (Figure 1a). The EARS is composed of two active rift axes: the magma-rich Eastern Branch, which defines the Somalian-Victoria plate boundary, and the magma-poor Western Branch, which delineates the Nubian-Victoria plate boundary. The Nubian-Victorian plate boundary is collocated with a zone of high seismicity west of the EARS Western Branch, including multiple Mw > 5 earthquakes. Thus, seismic hazards exist in the region, albeit at a low level (Delvaux et al., 2017; Poggi et al., 2017). This wide region of seismicity extends >170 km westward toward the Congo Craton, outboard the previously proposed Western Branch rift axis, and into the Luama-Kamituga Rift Zone (Figure 1b). The rift zone is a network of two contiguous

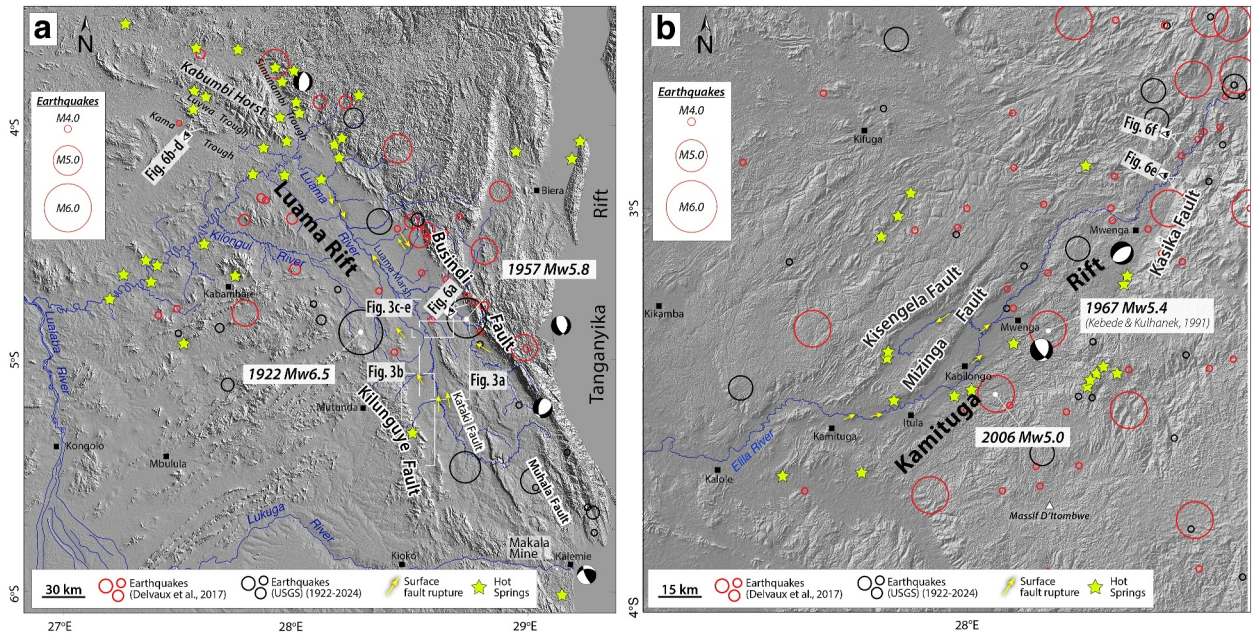

Figure 2. Shuttle Radar Topography Mission-Digital Elevation Model hillshade maps of (a) Luama Rift and (b) Kamituga Rift showing earthquakes, moment tensors (Ekstrom et al., 2012), surface rupture scarps, and hot springs (Delvaux et al., 2017; Veatch & Geological Society of America, 1935).

poorly studied rift basins: the NW-trending Luama Rift and the NE-trending Kamituga Rift, eastern DRC. The adjacent Tanganyika and Kivu Rifts are considered active rifts that delineate the Western Branch rift axis, while the Luama Rift and Kamituga Rift are commonly characterized as inactive rifts, with the Luama Rift considered a "failed" rift (Figure 1a). Failed rifts, or aulacogens, such as the well-studied Mid-Continent Rift and the Southern Oklahoma Aulacogen, are continental rifts that did not develop into seafloor spreading centers. Successful rifts will eventually evolve into an ocean basin, but will commonly undergo multiple cycles of "failure" and reactivation before break-up (e.g., Brune et al., 2023).

2.2.1. The Geology of the Luama and Kamituga Basins

The Luama Rift is a >250 km-long and 40–60 km-wide graben that hosts several hot springs and large earthquakes (Mw > 5, Figure 2a). The basin is bounded by the Busindi and Kilunguye border faults and hosts the Kataki and Muhala intrarift faults, first identified by Veatch and Geological Society of America (1935). The basin initially developed during the Permo-Triassic (Karoo) phase of rifting (e.g., Delvaux, 2001) and was later reactivated by extensional tectonics in the Cretaceous (Roberts et al., 2010, 2012). As such, the Luama Basin is composed of syn-rift Karoo sediments (Figure 1c). The Luama Rift has been identified as coeval, collinear, and parallel to the Rukwa Rift, with both basins being part of the NW-trending Karoo-age "Rukwa Trend" (Kolawole, Phillips, et al., 2021). The Chisi Shear Zone has been inferred as the boundary between the Kibaran and the Ruzizian-Ubendian Belts in the rift (Kolawole, Phillips, et al., 2021).

The Kamituga Rift is a basin that is approximately 100 km long and 20 km wide (Figure 2b). The basin does not appear to have a delineated, continuous border fault. Instead, the southern section of the Kamituga Rift hosts two large synthetic faults, the Kisengela and Mizinga Faults, and the northern section of the Kamituga Rift hosts the large Kasika Fault. The rift basin is dominated by Quaternary volcanics and siliciclastic sediments in floodplains of the Elila River, either directly overlying the Precambrian crystalline basement or underlain by Carboniferous-Permian glacial deposits (Figure 1c; Laghmouch et al., 2018). The Carboniferous-Permian deposits are widespread, generally occurring as NW–SE trending exposures, and are cross-cut by Quaternary faults (Figure 1c). The absence of mapped fault-bounded Karoo deposits indicates that the Kamituga Rift initiated in the Cenozoic, further supported by Kampunzu et al., 1998. The volcanism in the region occurs in two volcanic provinces: the Bukavu Volcanic Province, located in the southern section of the Kivu Rift, and the Mwenga-Kamituga Volcanic Province, located ~50 km farther southwest of Bukavu and is confined to the northern section of the Kamituga Rift (Figure 1c). The Mwenga-Kamituga Volcanic Province is dominated by basaltic volcanics, emplaced around

5.8–2.6 Ma with three distinct stages of fissure eruptions (Kampunzu et al., 1998). The first volcanic cycle occurred prior to the onset of the Kamituga Rift subsidence, while rift development took place between the first and second volcanic cycle (ca. 4–3 Ma). The Kamituga Rift has been interpreted as having initiated during the early stage of rifting, along with the rest of the Kivu Rift, but abandoned in a later stage when the active rift migrated eastwards to the newly formed N–S trending Rusizi depression, south of Lake Kivu (Delvaux et al., 2017, 2022). The Kamituga Rift has been regarded as the southwestern continuation of the Kivu Rift, given that both rifts are collinear and share a common Neogene magmatic history (Delvaux et al., 2017).

In general, the Phanerozoic tectono-stratigraphy of the Luama and Kamituga basins can be grouped into the known tectonic events that are recorded in many basins in East Africa. The Carboniferous-Early Jurassic units (they are fault-bounded in the Luama Rift) correspond to the earliest phase of tectonic extension in eastern Gondwana, popularly known as the "Karoo rifting event" (Castaing, 1991; Delvaux, 1989; Kolawole, Phillips, et al., 2021; Kolawole et al., 2022; Macgregor, 2017; Morley et al., 1999; Ring, 1995). Although this rifting event was concurrent with the development of a convergent plate boundary zone in South Africa (the Foreland Karoo Basin and the Cape Fold-Thrust Belt; Ring, 1995), many of the intracontinental rift basins experienced basin inversion leading to the failure of the rift basins in the Early Jurassic (e.g., Macgregor, 2017). In this contribution, we refer to this Early Mesozoic phase of tectonic extension in East Africa as "Rift Phase 1" (RP1; Figure 1c). The Luama Basin records mappable deposits of Cretaceous sediments, primarily confined to the hanging walls of the Kataki Fault, and corresponds to the Late Jurassic-Early Cretaceous rifting event in East Africa, recorded in many Karoo rift basins, and marking a reactivation of the Karoo basins (e.g., Castaing, 1991; Kolawole et al., 2022; Macgregor, 2017); herein referred to as "Rift Phase 2" (RP2). East Africa has been experiencing another phase of tectonic extension, which was initiated in the Miocene-Oligocene (e.g., Macgregor, 2015; Roberts et al., 2012), herein referred to as "Rift Phase 3" (RP3).

2.3. The Modern Geomorphology of the Luama and Kamituga Rifts

The modern landscape of the Luama Rift is drained by the Luama River (Figure 2a). The north-flowing, <400 km-long Luama River is the axial stream of the basin and is a large tributary of the Lualaba River, one of the major rivers in the DRC. The stream has five sources in the mountainous rift flanks, with two rising at altitudes >2 km (Bernacsek et al., 1992). In the river's lower course, the river descends three waterfalls and several minor rapids, but upstream, the basin tilts toward the Kataki Fault, and drains into a flat swampy valley which hosts a wetland system known as the Luama Marsh, ca. 100 km in length and covering ca. 600 km^2 (Figure 1d; Bernacsek et al., 1992). Toward the Kataki Fault, there is an active depocenter where incising channels are eroding the Mesozoic syn-rift sediments (Figure 1d). Veatch and Geological Society of America (1935) also documented extensive alluvial deposits in the southern part of the basin and at least two lake stages in the rift valley. The modern landscape of the Kamituga Rift is drained by the <250 km-long west-flowing Elila River (Figure 2b), which is also a large tributary of the Lualaba River. In both sub-basins, the bounding surfaces tilt toward the faults, and in the northern section of the Kamituga Rift, incising channels are eroding the volcanic sediments (Figure 1d).

3. Data and Method

In this study, we integrate topographic analysis, displacement distribution, slip tendency analytical techniques, and fault length scaling along the Luama and Kamituga Rifts. The work presented is primarily focused on satellite-based observations due to limited access to the study area, which was afflicted by an ongoing conflict in the DRC at the time of this study.

3.1. Evaluation of Large-Scale Rift Morphology Using Topography Data

The first-order variations in topographic relief patterns across and along rifts provide key insights into the rift structure, relationships between crustal deformation via subsidence and uplift domains, and surface processes (e.g., Gawthorpe & Leeder, 2000; Jackson et al., 2005; Kolawole, Firkins, et al., 2021; Kolawole, Phillips, et al., 2021; Laó-Dávila et al., 2015). We assess the topographical roughness to understand the morphology of the Luama and Kamituga Rifts. We divide each rift into 10 boxes and measure west-to-east topographic elevation profiles using a one-arc-second (30 m resolution) Shuttle Radar Topography Mission (SRTM)-DEM. The topographic profiles are 70 km long for the Luama basin and 40 km long for the Kamituga basin, spaced every

2 km, with sampling of elevation every 2 m. We stack each profile in each boxed area to obtain the sequential topographic characterization along each rift. We then compute the power spectral distribution (PSD) from each profile stack using a fast Fourier transform to quantify topographic roughness. We first remove the trend from the profile, truncate the profile or add zeros to make the total length an integer power of two, then taper the resulting sequence with a 10% cosine taper to reduce leakage from the side lobes of each spectral estimate (Bendat & Piersol, 2011; Brown & Scholz, 1985). The largest wavelength is the length of the profile, which is 70 km for the Luama basin and 40 km for the Kamituga basin, respectively. The smallest wavelength possible is 4 m, which is twice the sample interval. The apparent flattening of the largest wavelengths (i.e., the lowest spatial frequencies or wavenumbers) is an artifact of the measurement process. The removal of the profile trend forces the power at zero frequency to be zero; therefore, all spectra will roll off rapidly at low frequencies (Brown & Scholz, 1985). We describe one profile as smoother than another if its power spectral density is higher at longer wavelengths.

3.2. Fault Mapping in the Luama and Kamituga Rift Basins

We map fault traces using the SRTM-DEM, along with multi-resolution satellite images from Google Earth (CNES/Airbus, up to 50 cm spatial resolution) and legacy geology maps (e.g., Choubert & Faure-Muret, 1987; Veatch & Geological Society of America, 1935). We construct a hillshade map from the SRTM-DEM data to outline and trace fault surface expressions using ArcGIS software and classify each fault into two distinct categories based on geomorphic criteria: potentially active faults and other faults. As no active faults have been previously documented in the Luama-Kamituga Rift Zone, we utilize legacy geological maps to initially identify faults, including the Busundi and Muhala border fault system, the Kataki intra-rift fault, and two hot spring locations in the Luama Basin, as mapped by Veatch and Geological Society of America (1935). We then used geomorphic criteria to determine whether a fault has recently formed a scarp via offset of Quaternary surfaces implying that it is active (e.g., Burbank & Anderson, 2013). We delineate fault dip direction to be in the direction of surface subsidence that is sediment-hosted depocenters in the subsiding hanging wall adjacent to the fault trace.

We identify active faults based on evidence of displacement during the Quaternary period, as recent fault displacement tends to preserve more clearly defined surface scarps compared to those faults that moved in earlier geologic times (e.g., Kolawole et al., 2022; Williams et al., 2022). We classify faults as active by the presence of rectilinear, continuous, steep scarp along the base of a footwall escarpment (Figures 3a and 3b). Additional geomorphic criteria include offset Holocene surfaces, sharp surface expression with adjacent depocenters, control of river geometry and disruption of river paths, abrupt truncation of active channels and bounding actively subsiding swamp, and active hot springs (Figures 3c–3e). Although fault scarp degradation rates are not well constrained, studies of Mesozoic rifts with similar fault scarps indicate that inactive faults have experienced significant degradation since they were last active, approximately 65 million years ago (e.g., Kolawole et al., 2022; Ring, 1995; Wedmore et al., 2024). As the Luama and Kamituga Rifts are located in a tropical, humid climate that typically promotes erosion, the presence of well-preserved, continuous, sharp fault scarps with minimal degradation strongly supports recent (Quaternary) fault activity. We also combine the active fault mapping with United States Geological Survey (USGS) earthquake catalog data from 1922 to 2024 to examine geomorphic expression from recent earthquake ruptures (Figure 2). For the other faults, which are inferred to be inactive, the primary geomorphic criteria are the presence of degraded scarps and erosional features. Our use of the "inferred" designation is due to the uncertainty of whether the faults might be actively slipping at a lower rate than scarp erosion is occurring. We developed an ArcGIS digital fault database for the Luama and Kamituga Rifts, which is available in the Supporting Information S1, using the geomorphic criteria described above.

3.3. Field Ground Truthing of Active Rifting

Due to the long-standing civil conflict in the eastern DRC, we are unable to conduct extensive ground-based fieldwork. However, we examine the surface manifestation of active rifting along the rift zones, using aerial photography, and a few ground-based field observations (see locations in Figure 2). In the Luama Rift, we provide rift landscape observations from the southern (near Kalonda-Kibuyu) and northern (in Namoya) sections of the rift basin, including outcrop exposures and cores of Mesozoic syn-rift units at the Namoya Mine in Namoya. In the Kamituga Rift, we provide aerial photography taken on a flight from Bukavu to Namoya. We also assess rift morphology at the southwestern tip of the Kivu Rift, where the rift transitions into the northern section of the Kamituga Rift, as well as in the Kilombwe half-graben in the western margin of the Tanganyika Rift, north of the Luama Rift.

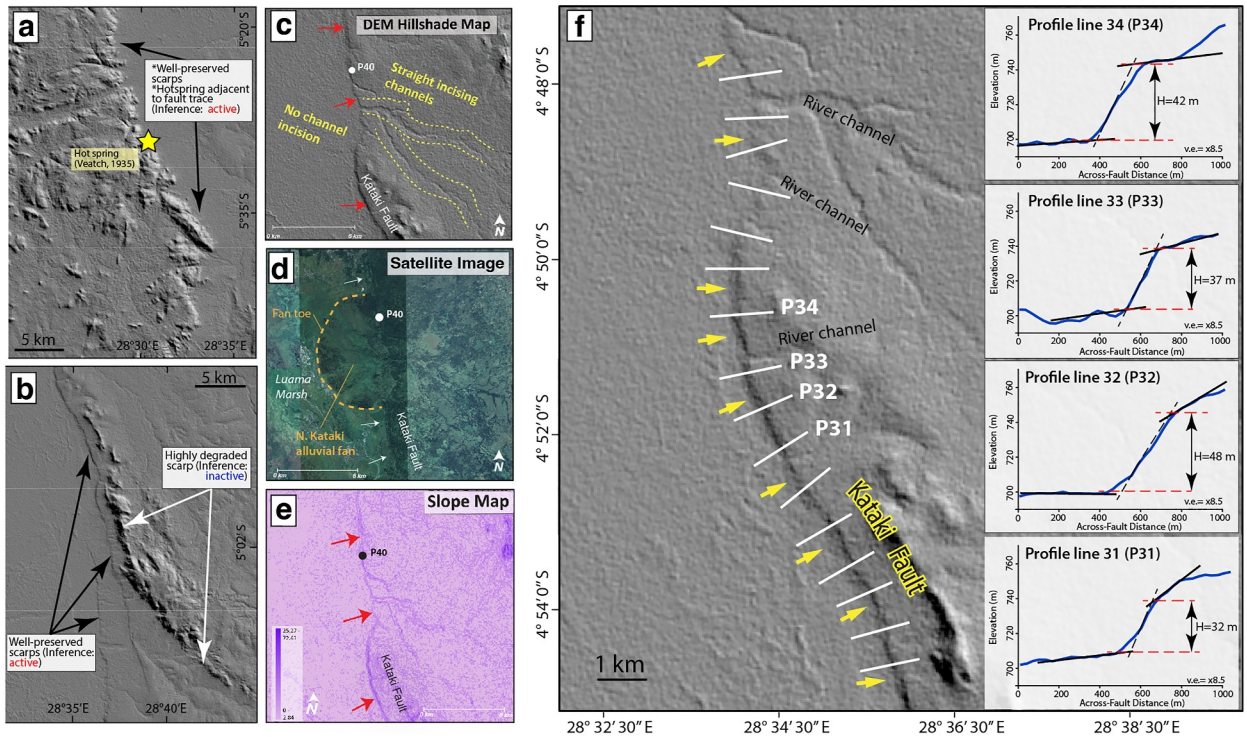

Figure 3. Illustration of the methods for geomorphic characterization of active faulting in the Luama-Kamituga Rift Zone and displacement distribution. (a, b) Examples of active and other scarps (i.e., those that are "potentially" inactive), showcasing some of the criteria for active fault characterization. (c–e) Shuttle Radar Topography Mission-Digital Elevation Model hillshade, satellite, and slope maps of the Kataki Fault showing >90 km-long fault scarps that deform the modern surface, and other geomorphic indicators of active footwall uplift. P40 is the profile number for the displacement distribution. (f) Local footwall relief (H) measurement along the Kataki Fault with example profile lines P31–P34. Yellow arrows indicate the Kataki Fault scarp. The insets show profile line examples; the black solid line represents the regression fit to elevations in the footwall and hanging wall, the black dotted line indicates the maximum slope steepness of the scarp, and the red dotted lines represent the vertical differences between the extrapolated regression lines at the maximum steepness on the scarp—all profile locations in Figure S1 of Supporting Information S1.

3.4. Measurement of Displacement Distribution on Selected Large Faults

To understand how the displacement distribution relates to the source of the stress field, we measure the surface displacement distribution of the fault scarp, which indicates the most recent slip on a normal fault. We focus the measurement of displacement distribution on the Luama Rift due to the hard-linkage of the basin with the adjacent Tanganyika Rift, a characteristic that is lacking in the Kamituga Rift (lacks hard-linkage with the Kivu Rift, its closest known rift). We measured along-fault scarp height using the SRTM-DEM of the two most prominent faults in the Luama Rift: the Busindi Fault, which is the north–east bounding fault, and the Kataki Fault, which is the largest intra-rift fault in the basin. This allowed us to compare the slip distribution in the border area of the basin with that in the central regions of the basin. We extracted ∼1 km-long fault-perpendicular topographic profiles every 1 km, carefully avoiding geomorphic indicators that might not be representative of the fault scarp (e.g., river channels). We measured the local footwall relief (H) by fitting regression lines to the footwall and hanging wall topography of the profiles and calculating the vertical difference between the extrapolated regression lines at the maximum steepness on the scarp (Figure 3f; Avouac, 1993). We filter the resulting measurements along-strike using a 4-km-wide moving median.

3.5. Assessment of Contemporary Stress Field From Earthquake Focal Mechanisms in the Kamituga Rift

We perform stress inversion to study the contemporary stress field of the Kamituga Rift using a similar approach to that of Delvaux and Barth (2010) and the methodology described in Delvaux and Sperner (2003). Stress inversion is not possible in the Luama Rift due to unavailable focal mechanisms in the basin itself (Figure 2a). We used the Win-Tensor program (Delvaux, 2011, 2012) to input the given earthquake focal mechanism solutions located in the Kamituga Rift (Table S1 in Supporting Information S1, locations shown in Figure 2b). The stress

inversion method (Angelier, 1989; Angelier & Mechler, 1977) determines a reduced tensor which contains the orientations of the principal compressive stress axes (σ_1, σ_2 and σ_3, where $\sigma_1 \geq \sigma_2 \geq \sigma_3$), and the stress ratio R $(\sigma_2 - \sigma_3)/(\sigma_1 - \sigma_3)$ which expresses the relative stress magnitude. The Win-Tensor program first estimates the tensor solution using the Right Dihedron Method to determine the range of possible orientations for σ_1 and σ_3. Next, the iterative grid-search Rotational Optimisation procedure is used with the initial tensor result as a starting point. We used the misfit function in Win-Tensor (described as f3 in Delvaux & Sperner, 2003; F5 in Win-Tensor) to minimize the misfit difference between the calculated slip direction and the resolved direction (α). The misfit function is independent of the ratio σ_3/σ_1 and favors higher shear stress magnitudes and lower normal stress magnitudes on the plane, promoting slip. The type of stress regime is also illustrated in Frohlich's triangular diagrams (Frohlich, 1992). Every tensor obtained is associated with a quality rank parameter, which ranges from A to E (A for very good, B: Good, C: fair, D: poor, E: very poor) as defined in Delvaux and Sperner (2003), with D-quality and below considered poorly constrained and unstable. Following Delvaux and Barth (2010), we first inverted the focal mechanism data (Table S1 in Supporting Information S1) using both nodal planes, treating them as independent data, to obtain a stress tensor. Due to the relatively limited number of focal mechanisms, we did not remove any nodal planes from the inversion as the misfit angle did not exceed 30°.

3.6. Quantitative Assessment of Reactivation Tendencies of the Mapped Faults

We assess the reactivation potential of the mapped active faults under a given stress field (Morris et al., 1996). Slip tendency analysis has been successfully employed to characterize the likelihood of fault slip in stress regimes associated with normal faulting (e.g., Ferrill et al., 1998; Nkodia et al., 2022). Due to the lack of available computed stress fields for the Luama and Kamituga Rifts, we test the stress tensors obtained from the surrounding contemporary EARS stress fields and examine their respective likelihood to reactivate the mapped active faults. As the Luama Rift is adjacent to the Tanganyika Rift, we test the north and south Tanganyika Rift stress fields from Delvaux and Barth (2010) and the south Tanganyika Rift stress field obtained from teleseisms recorded between 1977 and 2017 by Lavayssière et al. (2019). For the Kamituga Rift, we test the Kivu stress field from Delvaux and Barth (2010). We also perform a stress inversion with the available earthquake focal mechanisms in the basin (described in Section 3.5). The principal compressive stress axes and stress ratios for each regional stress field are listed in Table S2 of Supporting Information S1.

Fault reactivation potential assesses the susceptibility of a fault, given its orientation and stress state, to slip under the Mohr-Coulomb criterion. Frictional sliding on a pre-existing fracture occurs when the shear stress, σ_s, on the plane exceeds its shear strength, σ_f. Frictional sliding also depends on the cohesion, C, the friction coefficient $\mu = \tan \varphi$ (where φ is the angle of internal friction), and the effective normal stress on the plane, σ'_n (e.g., Angelier, 1989), such that:

$$\sigma_s \geq \sigma_f = C + \sigma'_n \tan \varphi = C + \sigma'_n \mu \quad (1)$$

Following Morris et al. (1996), the slip tendency, Ts, is the ratio of maximum resolved shear stress, σ_s, to normal stress σ_n acting on a fault or fracture surface under a given stress field:

$$Ts = \sigma_s/\sigma_n \quad (2)$$

The normalized slip tendency, TsN, that is, values between 0 and 1, is obtained by normalizing the Ts values to their maximum value, that is, $\mathrm{TsN} = \frac{Ts}{\max(Ts)}$.

For a fault to slip and reactivate, Ts must lie above the lines of initial friction defined by its coefficient of friction $\mu = \tan \varphi$. The effective coefficient of friction (μ') describes the maximum value of μ or the lowest value of pore fluid pressure that allows faults to reactivate for a given stress state, without also inducing failure along optimally oriented planes in intact rock. We use cohesion C = 20 MPa and $\mu' = 0.55$, which Williams et al. (2019) obtained in their study of fault reactivation in southern Malawi. We use a dip of 60°, based on the average fault dips at the Makala coal mine in the Luama Rift (location shown in Figure 2a, near Kalemie; Tshibangu & Descamps, 2016).

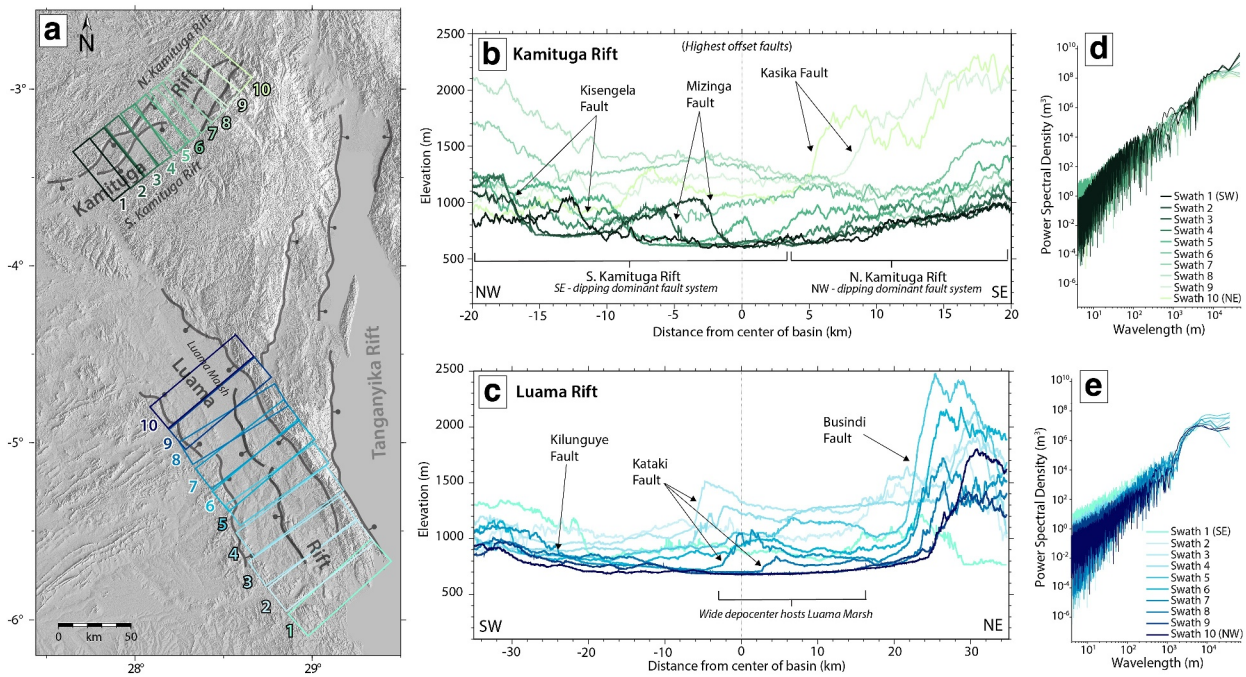

Figure 4. Topographic characterization of the Luama-Kamituga Rift Zone. (a) Shuttle Radar Topography Mission-Digital Elevation Model hillshade map with 15 km-wide, color-coded boxes along each rift from which topographic profiles were extracted west to east. (b) NW to SE 40-km-long stacked topographic profiles for the Kamituga Rift. (c) SW to NE 70-km-long stacked topographic profiles. (d, e) Power spectral density for three topographic profile stacks in the Kamituga Rift and Luama Rift. A profile is smoother than another if its power spectral density is higher at longer wavelength. The morphology of the Luama Rift becomes rougher toward the Tanganyika Rift, while the Kamituga Rift shows similar roughness across the rift.

3.7. Statistical Test of Fault Length Distribution

The spatial distribution of faults and the empirical fault length distribution provide a basis for evaluating the phases of rift maturity (e.g., Grant et al., 2024; Gupta & Scholz, 2000; Michas et al., 2015; Williams et al., 2022). We analyze the mapped faults using a statistical test to quantify the distribution of fault lengths in the Luama-Kamituga Rift Zone. We test two groups of fault length data, the mapped active faults in the Luama Rift and the Kamituga Rift, respectively, to investigate the rift evolution phase of each basin. We follow the methodology described by Williams et al. (2022) and Grant et al. (2024) and use a two-sample Kolmogorov-Smirnov (KS) test to determine whether the fault length data can be described by a power-law or exponential distribution (Clauset et al., 2009; Massey, 1951). We first use a Maximum Likelihood Estimator to fit a power-law and exponential function to the data. Next, we apply the two-sample KS test to determine whether the empirical data, which is the observed fault length frequency distribution, can be considered a random sample from the theoretical distribution. The theoretical distribution expresses the probability that a random variable L is greater than or equal to the fault length l using the exponent α from the power-law fit and the rate parameter λ from the exponential fit. l_{min} is a lower bound used to estimate α, and λ is used to account for the length below which the fault mapping is considered incomplete. Following the criteria in Grant et al. (2024), we determine l_{min} by considering where the cumulative length data begins to deviate from the broader trend that it maintains throughout the rest of the plot. We choose the lowest fault length cutoff $l_{min} = 5$ km and $l_{min} = 10$ km for the Kamituga Rift, and $l_{min} = 10$ km and $l_{min} = 15$ km for the Luama Rift.

4. Results

4.1. Rift Basin Morphology Along the Luama and Kamituga Rifts

To evaluate the first-order patterns of active tectonics, we characterize the rift morphology using the topographic stacked profiles along each rift (Figures 4a–4c). The Kamituga Rift along-rift changes in rift morphology are characterized by the flip in fault polarity from SE-dipping faults and a large intra-rift fault to the SW, to NW-dipping faults and large intra-rift faults to the NE (Figure 4b). Based on this distinct character, the Kamituga

10.1029/2025TC008815

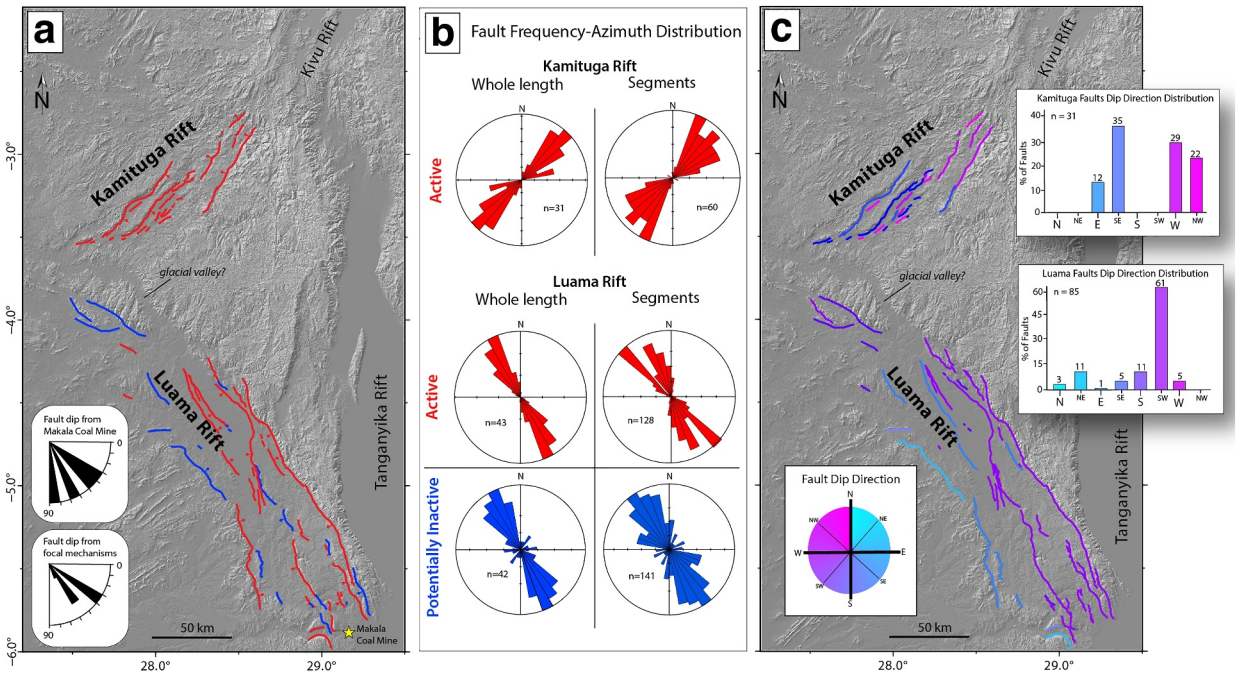

Figure 5. Fault distribution of the Luama-Kamituga Rift Zone. (a) Shuttle Radar Topography Mission-Digital Elevation Model hillshade map of the study area overlaid with our updated faults color-coded by their inferred status as either active or inactive. (b) Frequency-azimuth distribution of the mapped faults grouped into active (red) and inactive (blue), for the whole length and segments of the faults. The segmentation for the rose plot is based on geometrical changes along the faults. (c) Distribution of fault dip-direction.

Rift is composed of two sub-sections: North and South Kamituga Rift. For the Luama Rift, the rift morphology is defined by the dominant SW dipping border fault (Busindi Fault) polarity, which remains uniform along-strike of the rift (Figure 4c). Intrarift faulting (e.g., Kataki Fault) accommodates more strain in the central region of the rift basin and decreases northwards. Furthermore, our qualitative assessment of topographic relief "roughness" at the scale of the rift basins reveals systematic along-rift variations in calculated power spectrum densities (Figures 4d and 4e). The power spectra for the Kamituga Rift (Figure 4d and Figure S2 in Supporting Information S1) mostly overlap indicating that relief "roughness" is generally similar along the rift, but with the longer wavelength relief dominating in sections where active fault scarps are less prominent (i.e., northern segment of the rift and in the transfer zone between the northern and southern rift segments), indicating less erosion and depocenter development (Figures 4a and 4b). For the Luama Rift (Figure 4e and Figure S2 in Supporting Information S1), the longest wavelength relief signals are most dominant in the NE segment of the rift, where the basin hosts the Luama Marsh, highlighting more vigorous erosion and depocenter development.

4.2. Distribution of Active Faulting in the Luama Rift and Kamituga Rifts

We mapped 85 faults for the Luama Rift, of which 43 are potentially active (Figure 5a). The active fault orientations show a narrow unimodal distribution in strike (130°–160°). In contrast, the inferred inactive faults exhibit a wider range and multimodal distribution in strike 30°–40°, 80°–90°, and 140°–160° (Figure 5b). We also examined the fault segment orientations based on fault geometry, with 128 active fault segments and 141 inferred inactive fault segments. The frequency-azimuth distribution for fault segments orientation yields a similar pattern to the whole-length fault orientation, with active fault segments exhibiting a broadly unimodal range of 120°–185° and inferred active faults exhibiting a multimodal distribution in strike, with wider ranges of 0°–20°, 50°–60°, and 100°–180° (Figure 5b). The dominant distribution of dip directions is SW and W, with 45% and 29% of the faults respectively, with the remaining fault dip direction being broadly distributed (Figure 5c). We mapped 31 faults for the Kamituga Rift, of which the dip direction distribution is NW for 51% of the faults and SE for 48% of the faults. The fault orientations show a narrow unimodal distribution in strike, in the range of 40°–60°, and a slightly broader range of 30°–80° for the active fault segments (Figure 5b). The dip direction is predominantly SE and W/NW (Figure 5c).

10.1029/2025TC008815

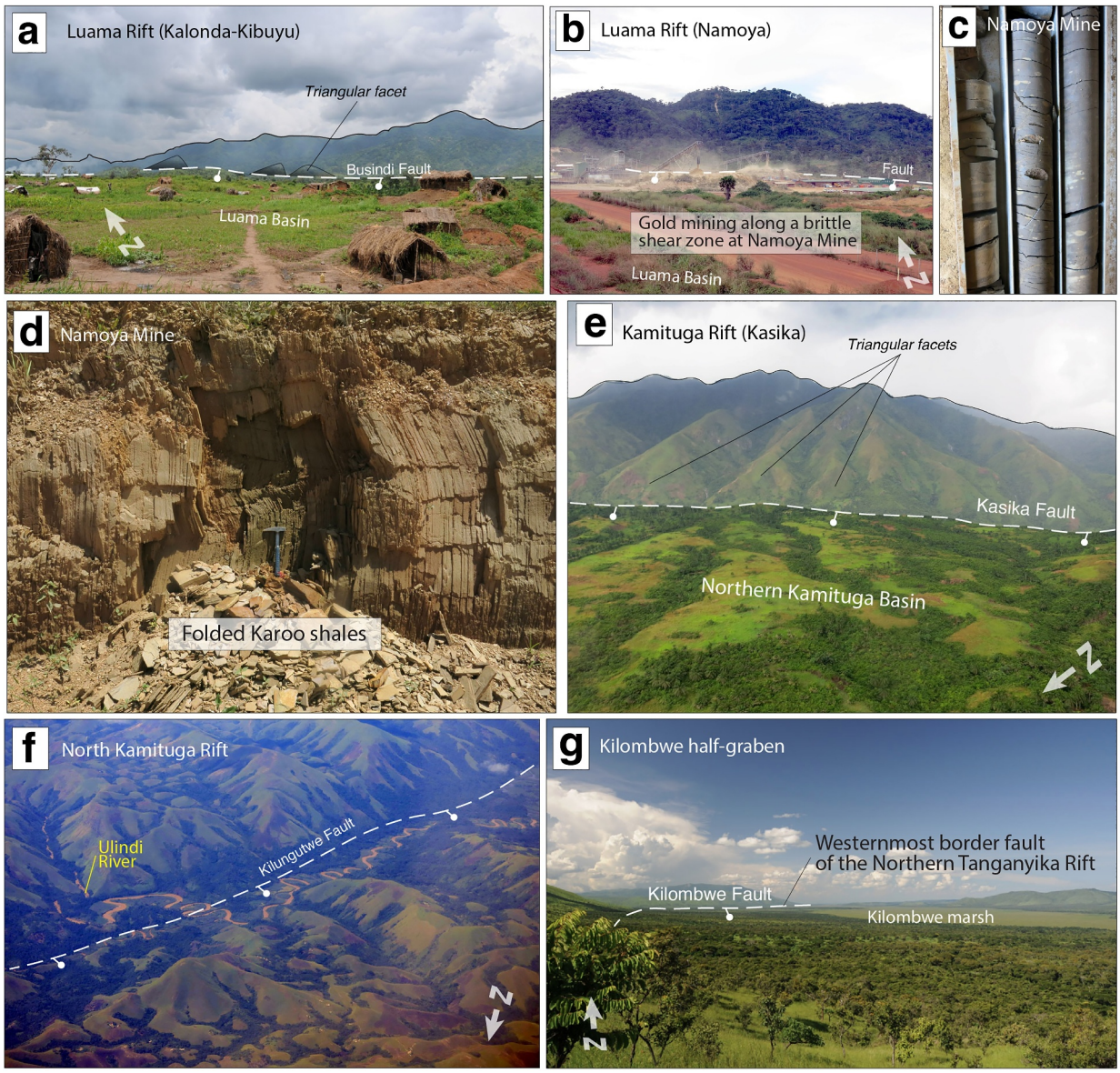

Figure 6. Ground-truthing the Luama-Kamituga Rift Zone. (a) Photograph looking north toward the Busindi Fault near Kalonda-Kibuyu (courtesy of Stefan Roman; German Society for International Cooperation). (b) Namoya Mine in the Luama Basin. (c) Core from Namoya Mine. (d) Karoo outcrop in Namoya Mine. (e) Kasika Fault, Kamituga Rift. (f) Kilungutwe Fault, Northern Kamituga Rift. (g) Kilombwe Fault, defining the westernmost border fault of the northern Tanganyika Rift. Note the depocenter basin morphology and wetland development on the Kilombwe Fault hanging wall (courtesy of Stefan Roman; German Society for International Cooperation).

In the field, the escarpment of the Busindi Fault exhibits triangular facets, indicating active uplift of the footwall (Figure 6a). The Namoya Gold Mine, located along a fault scarp near the northern end of the Luama Rift, exploits hydrothermal gold mineralization that was found along a brittle shear zone (Figures 6b–6d; location in Figure 2a; Wakenge & Matthysen, 2023). At the mine, core samples (Figure 6c) and field outcrops (Figure 6d) reveal the presence of tilted Karoo shales on the hanging wall. The tilted Karoo units are sub-vertical with superposed secondary folds on a larger limb (Figure 6d). In the Kamituga Rift, we observe the presence of triangular facets at the base of the Kasika Fault scarp in the northern Kamituga Rift, with transitions from linear incisive Ulindi River channels in the footwalls to sinuous channels in the hanging walls of the Kilungutwe Fault, all indicating active fault slip and footwall uplift in the areas (Figures 6e and 6f). Similarly, in the Kilombwe Half-graben in which the Kilombwe Fault bounds exposures of Karoo sediments (Figure 1c), we observe prominence of the fault scarp, "depocenter" basin morphology with wetland development on the Kilombwe Fault hanging wall (Figure 6g).

4.3. Distribution of Surface Displacement Along Prominent Surface Fault Ruptures

We measured 133 displacement profiles along the 172 km-long NW-trending Busindi Fault (Figure S3a in Supporting Information S1). The distribution of displacement along the border fault shows that the fault is subdivided into five main composite fault segments (CS). The southernmost segment and closest to the Tanganyika Rift is the Southern CS, with the shortest length of 9 km. The Central CS is 70 km long with a maximum local footwall relief of 133 m, which is also the maximum displacement of the Busindi Fault. The Northern CS is 21 km in length with a maximum local footwall relief of 100 m. The northernmost segments, Northern CS #2, which is 27 km long, and Northern CS #3, which is 16 km-long, have the lowest maximum local footwall reliefs in the Busindi Fault of 75 m and 65 m, respectively. We interpreted sub-segments in the Central CS and the Northern CS, with an average sub-segment length of 11.1 km, based on the locations of displacement minima along the moving median curve. The Central CS has eight sub-segments, and the Northern CS has 2. The segmentation index is nine sub-segments per 100 km.

The main intra-rift fault in the basin, the Kataki Fault, exhibits an identical distribution of displacement pattern to the Busindi Fault (Figure S3b in Supporting Information S1). We measured 99 displacement profiles along the 100 km NW-trending Kataki Fault. The fault is subdivided into three main composite fault segments. The southernmost segment is 55 km long and has a maximum local footwall relief of 47 m, the highest of the fault. The Central CS is 23 km in length and has a maximum local footwall relief of 22 m. The northernmost segment is 22 km long with a maximum local footwall relief of 8 m. The Southern CS is subdivided into four sub-segments, while the Northern CS is subdivided into two. The average sub-segment length is 14.1 km.

4.4. Contemporary Tectonic Stress and Resolved Reactivation Tendencies of the Luama and Kamituga Rifts

The stress inversion of the focal mechanisms (Figure 7a) yields a pure normal faulting stress regime ($R' = 0.50 \pm 0.16$). The maximum horizontal compressive stress (SHmax) orientation is NNE-SSW (N16E° ± 30°). The tensor quality is C (SHmax/SHmin within ±20–25°), indicating that it is fairly constrained. Nodal planes mostly strike NE–SW, with one plane striking NW–SE. The axis orientations of the stress tensor are σ_1 = 080/030, σ_2 = 009/196, and σ_3 = 002/286, with $R = 0.5$. The different stress fields applied to the fault systems mapped show that several faults are more likely to be reactivated in the Luama and Kamituga Rifts (Figures 7b–7f). For the mapped faults in the Kamituga Rift, we applied the adjacent Kivu stress field and the stress inversion results (Figures 7b and 7c). The focal mechanism solutions stress inversion (Figure 7b) show broadly lower TsN values than the Kivu stress field, with NE–SW striking and NW and SE dipping faults exhibiting high TsN values, indicating that these segments are the most likely to activate. For the Kivu stress field, most NE–SW striking and NW dipping faults show the highest TsN value, suggesting they can be reactivated, whereas SE dipping faults show a low TsN value (Figure 7c).

For the Luama Rift mapped faults, most of the NW–SE striking and SW dipping faults can be reactivated when applying North and South Tanganyika stress fields (Figures 7d–7f). The northern Tanganyika stress field (Figure 7d) shows the highest value of TsN (TsN = 90%–100%, red planes) across all three applied stress fields for NW–SE striking and SW dipping faults. The NW–SE striking and NE dipping faults, and the WNW-ESE oriented faults, show moderately low TsN values (TsN = 30%–60%, cyan-green planes). The lowest TsN value (TsN = 0%–20%, dark blue-cyan planes) corresponds to ENE-WSW striking faults. The ENE-WSW planes are misoriented for reactivation as they plot beneath the failure envelope in the Mohr diagram, which, together with the lowest TsN values, suggests that the faults could not be reactivated in such a stress field. For the southern Tanganyika stress field from Delvaux and Barth (2010), NW–SE striking and SW dipping faults also show a high TsN value (Figure 7e). Contrary to the North Tanganyika stress field, active faults striking NW–SE and dipping SE show a moderately high TsN value (TsN = 70%–80%, yellow-orange planes) while N–S striking active planes show a low TsN value. ENE-WSW planes exhibit a slightly higher TsN value but remain misoriented for reactivation in the Mohr diagram. For the second southern Tanganyika stress field obtained from Lavayssière et al. (2019), NW–SE striking and SW dipping faults show a high TsN value (Figure 7f). The WNW-ESE oriented faults show a moderately lower TsN value (TsN = 30%–60%), and NW–SE striking and NE dipping planes show a moderately high TsN value (TsN = 70%–80%, orange planes) compared to previous field stresses. Overall, the three contemporary EARS stress fields applied to the Luama Basin mapped faults show a broadly similar pattern: NW–SE striking and SW dipping fault segments show the highest TsN value, indicating that those fault segments

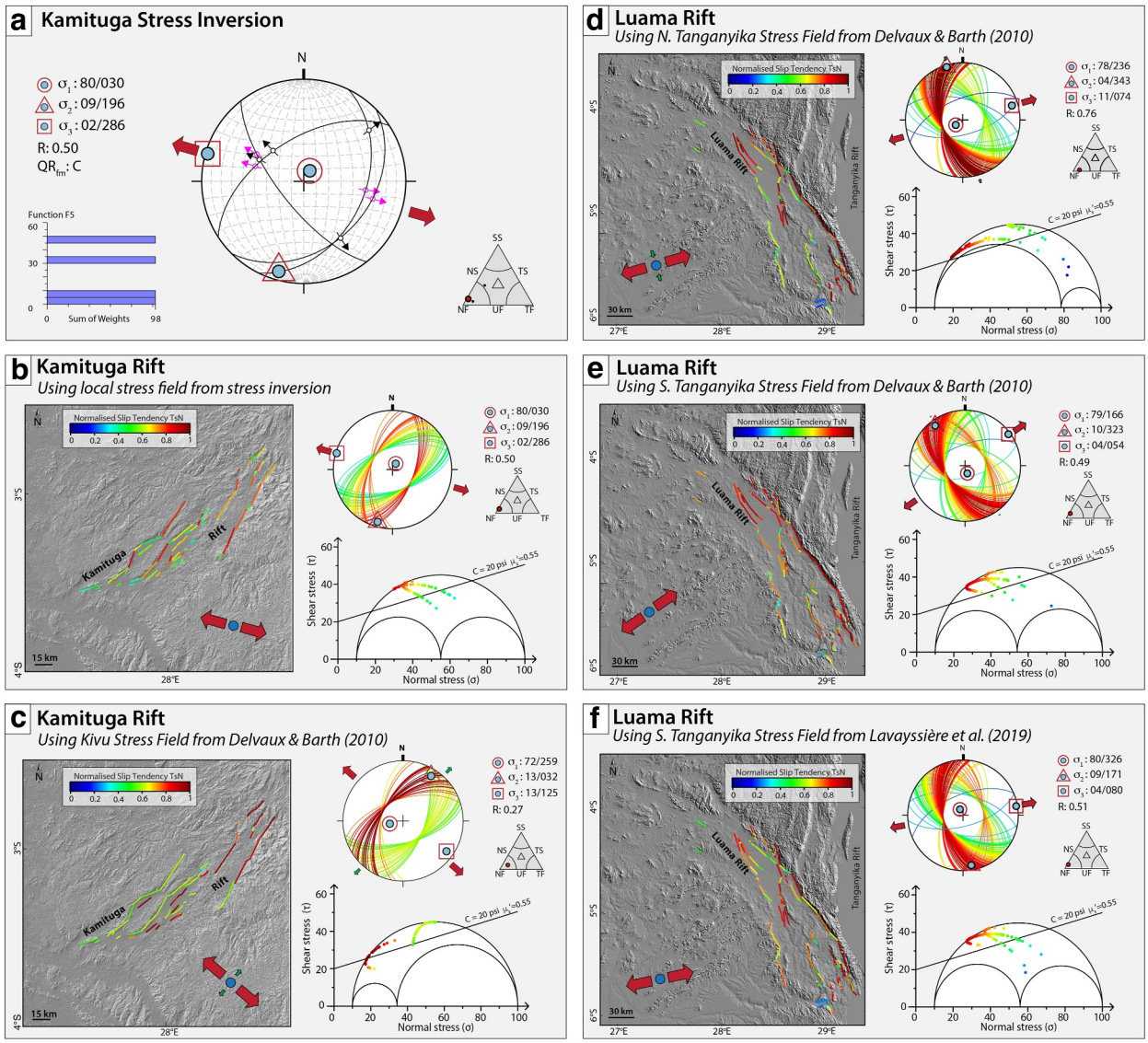

Figure 7. Reactivation tendency of mapped active faults in the Luama-Kamituga Rift Zone. (a) Kamituga Rift stress field from focal mechanisms solutions stress inversion (Delvaux, 2012). (b–f) Mohr-Coulomb plots and equivalent lower hemisphere stereographic projections of mapped active fault segments within the Kamituga Rift (b, c) and Luama Rift (d–f), color-coded by the inferred slip tendency in contemporary EARS stress field (i.e., stress fields at the Kivu and Tanganyika Rifts).

are the most likely to reactivate, and the ENE-WSW planes show the lowest TsN value, suggesting that those planes are misoriented for reactivation.

4.5. Fault Length Distribution in the Luama-Kamituga Rift Zone

We present new data on fault length distributions in the Luama and Kamituga Rifts. For the mapped faults in the Kamituga Rift, neither a power-law nor an exponential distribution can be rejected (Figures 8b–8e). In the p-value plot, the power-law fault length distribution cannot be rejected for any value of l_{min}. Similarly, the exponential cannot be rejected for any value of l_{min} for the range 6 km < l_{min} < 7 km, where the p-value is below 0.1 (Figure 8c). The exponential model shows a significantly poorer fit of survival function results but we cannot reject the null hypothesis (i.e., $p > 0.1$) (Figures 8d and 8e). We note that for $l_{min} = 10$ km, both the exponential and power-law distributions show a high p-value, with the power-law model remaining the best fit with the higher p-value (Figure 8e). However, the fault distribution for the $l_{min} = 10$ cutoff is not robust enough, as it only uses 10 faults.

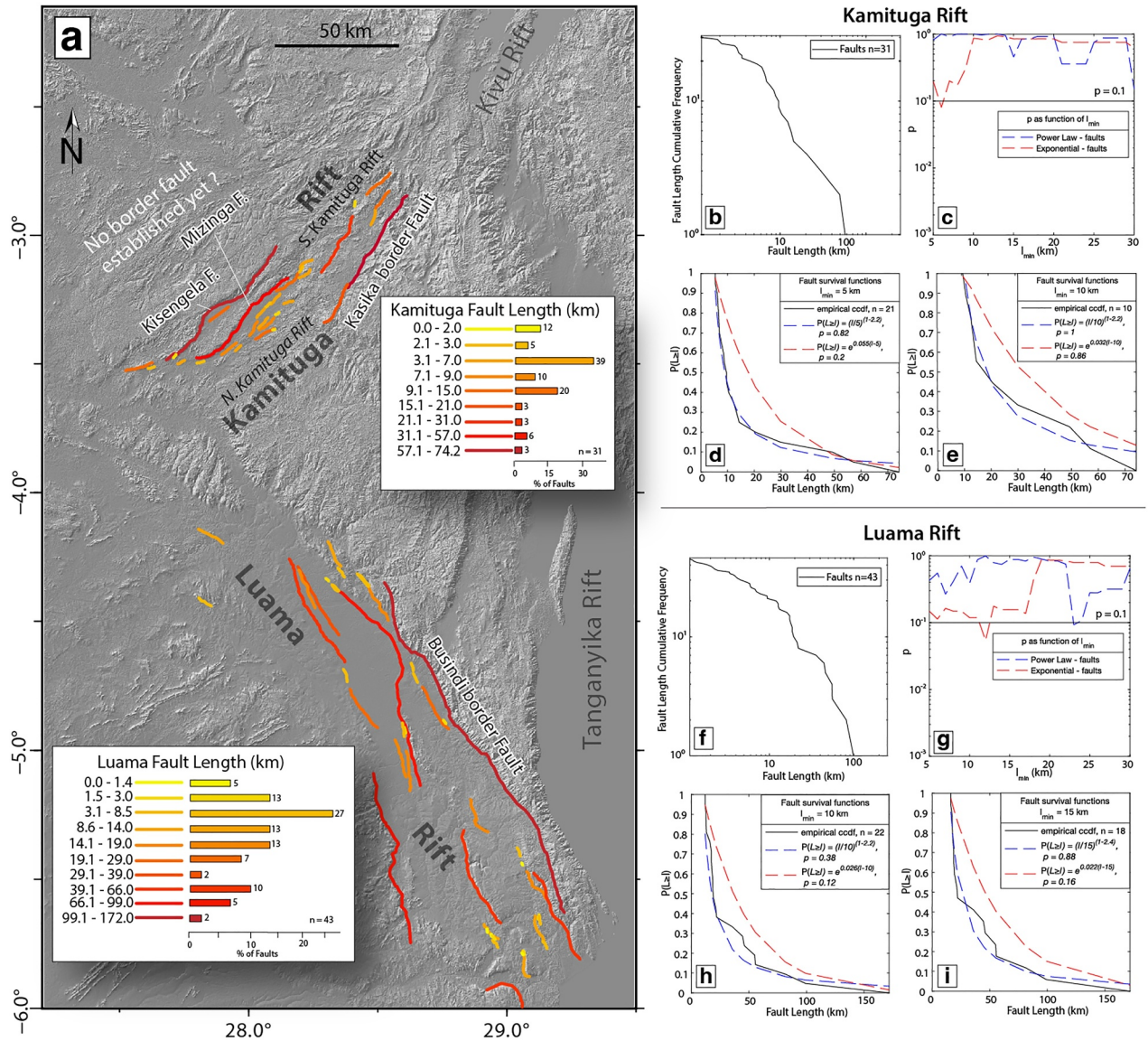

Figure 8. Fault length distribution statistics. (a) Shuttle Radar Topography Mission-Digital Elevation Model hillshade map of the Luama-Kamituga Rift Zone with mapped active faults color-coded by fault length. Insets: fault length histograms. Note the variable bin size to avoid gaps. (b–i) Statistical assessment of fault length distribution in Kamituga Rift (b–e) and Luama Rift (f–i). (b, f) Cumulative frequency of faults greater than or equal to a given fault length. (c, g) Probability (ρ) that the empirical data is a sample from the best-fit theoretical power law or exponential distribution. (d, e, h, i) Empirical and theoretical fault length survival functions from a two-sample Kolmogorov-Smirnov (KS) test for two different values of the lowest fault length cutoff (Kamituga Rift: l_{min} = 5 km and l_{min} = 10 km, Luama Rift: l_{min} = 10 km and l_{min} = 20 km). A higher cutoff would result in ß too few faults to make the results statistically robust. The black horizontal line represents the p-value (0.1) below which the KS test rejects the null hypothesis. The inset boxes show the equations for the theoretical trends and their fit to the empirical trend (i.e., the p-value from the KS test).

For the mapped faults in the Luama Rift, we cannot reject the null hypothesis that the empirical data is drawn from a power-law distribution for 10 km < l_{min} < 15 km (Figures 8f–8i). The exponential and power-law fault distributions are statistically significant ($p > 0.1$), so we cannot reject either model for any value of l_{min}, except for the range 11 km < l_{min} < 13 km for the exponential curve (Figure 8g). The exponential model shows a significantly poorer fit of survival function results compared to the power-law model, indicating that the power-law distribution is the best fit for the Luama Rift fault length distribution (Figures 8h and 8i).

5. Discussion

5.1. Incipient Activation of the Luama and Kamituga Rifts as Segments of the East African Rift System (EARS)

5.1.1. Surface Manifestations of Incipient Rifting and Incipient Reactivation of a Failed Rift

The presence of fault-bounded Karoo and Cretaceous deposits in the Luama Rift and Kilombwe Half-graben indicates that these rifts accorded tectonic extension in the Mesozoic (Figure 1b; Choubert & Faure-Muret, 1987; Laghmouch et al., 2018). However, our observation of oversteepened Karoo Shales in the Luama Rift (Figure 6d) suggests that the basin was inverted during failure in the Early Jurassic period. The Kamituga Rift was likely initiated in the Cenozoic as we do not find evidence of fault-bounded Mesozoic deposits in the basin, supporting the interpretation by Kampunzu et al. (1998). The Luama-Kamituga Rift Zone showcases attributes of an incipient tectonic rift undergoing reactivation. The rift basins host large earthquakes, such as the Mw 6.5 1922 earthquake. The sparseness of earthquakes is likely due to the limited number of seismic stations deployed in the basins. Despite the lack of seismic coverage, the rift zone has hosted more than 50 recorded earthquakes, indicating that the faults in the Luama-Kamituga Rift Zone are seismically active. The rift zone is also included in seismic hazard assessment maps (Delvaux et al., 2017; Poggi et al., 2017).

The first-order rift morphology pattern offers insights into the rift structure and surface processes of rifts. The Luama Rift morphology is dominated by the Busindi border Fault and the Kataki intrarift Fault, both of which have displacement increasing toward the south of the basin. We also observe evidence of concurrent reactivation of the Kataki Fault, as indicated by the presence of the N. Kataki alluvial fans (Figure 3d), suggesting active uplift. The topographic expression of the Luama Rift becomes rougher toward the south of the basin, adjacent to the active Tanganyika Rift, as indicated by the calculated power spectral densities (Figures 4d and 4e). We infer that the rougher topography indicates that more weathering is occurring due to the uplift of the rift flank. Consequently, the efficient weathering results in a geomorphologic expression that is characteristic of a transport-limited landscape. The Kamituga Rift morphology is characterized by the along-rift fault polarity flip from NW-dipping to SE-dipping toward the south of the basin, and the almost equally large Kisengela and Mizinga faults located in the middle of the rift. The topographic expressions for each profile are similarly rough along the Kamituga Rift, which could indicate a weather-limited landscape. Based on these observations, we interpret that a border fault has not been established across the Kamituga Rift, and the basin is divided into two sub-basins: the North Kamituga sub-basin and the South Kamituga sub-basin. The depocenter development is more prominent in the southern basin, indicating that the South Kamituga Rift is more developed. In the northern basin, tectonic faulting followed rift volcanics, as rift faulting is not pronounced in the hanging wall (in agreement with Kampunzu et al., 1998). Alternatively, faulting occurred concurrently with volcanic dike intrusion, with dikes absorbing most of the strain and thereby starving the faults of strain.

The distribution of the mapped fault scarps in the Luama and Kamituga Rifts, including a fault scarp exceeding 90 km in length, displays geomorphic indicators that suggest tectonic rift reactivation. The reactivated faults cut and offset the hummocky erosional landscape of the exposed Cretaceous sediments. The faults also disrupt streams by uplifting their upstream sections, causing them to down-cut and erode into the landscape of the fault footwalls, as indicated by the presence of triangular facets (Figures 6a and 6e). The spatial pattern of the mapped faults suggests that the active faulting in the basins is widespread.

The displacement distribution illustrates the segmentation and modern slip patterns along the Busindi and Kataki Faults, as well as their relationship to the stress field source. Overall, the Busindi Fault exhibits a greater intensity of segmentation and a greater maximum throw than the Kataki Fault. The broad trend illustrated by the moving median curves shows that both the Kataki and Busindi Faults exhibit a clear southward increase in throw magnitude toward the intersection of the basin with the Tanganyika Rift, the nearest known active plate boundary in the EARS. This displacement pattern suggests that there is increasing strain accommodation in the southeastern section of the basin, proximal to the East African Rift axis, indicating the control of the East African Rift tectonics on Cenozoic strain localization in the Luama Basin. All these observations suggest that the Luama and Kamituga Rifts are another previously unidentified yet active segment of the EARS.

5.1.2. Attributes of Active Rift Faulting and Implications for the Early Stage Plate Boundary Development Along the Luama-Kamituga Rift Zone

Fault length distribution in rifts depends on the magnitude of strain accommodated by faults and evolves with increasing strain, as demonstrated by statistical analyses of fault patterns in computational and experimental models (e.g., Cowie et al., 1995, 2005; Spyropoulos et al., 1999, 2002). Based on observation and experiments on cracks, strain magnitude controls fault length distribution, which transitions from exponential at very low strains, where fault nucleation prevails, to power law at low to intermediate strains, where fault growth prevails, and back to exponential when the largest faults develop at higher strains due to fault coalescence (Spyropoulos et al., 2002). Faults in continental rifts exhibit a similar pattern in terms of length distribution and evolution. Rifts initiate with an exponential fault length distribution and subsequently transition to a power-law distribution as the rift undergoes the stretching phase and strain migrates onto large inward-dipping faults (e.g., Grant et al., 2024). As the rift maturity evolves, the fault length distribution may later return to an exponential distribution (e.g., Gupta & Scholz, 2000; Michas et al., 2015; Williams et al., 2022). Our fault length attribute results show predominantly power-law distribution for both the Luama and Kamituga Rifts, indicating that fault length growth is occurring in the basins.

Along with fault length attributes, the dominant fault dip direction is key in strain localization during rift evolution, as strain localization dominates rift basin development and is manifested near the surface by a systematic migration of fault activity (Cowie et al., 2005). At rift initiation, both inward and outward-facing faults develop with similar low slip rates. As strain localizes onto large inward-dipping fault arrays, the outward-dipping faults become inactive, and the inward-dipping faults develop higher slip rates. Subsequently, strain migrates toward rift axes with strain rates at the eventual rift axis increasing, thus becoming the border fault of the rift while strain rates over the flanking areas decline. Our results in rift morphology (Figures 4b and 4c) and fault dip distribution (Figure 5c) indicates that the dominant fault dip for each basin is SW for the Luama Rift and NW and SE in the northern and southern sections of the Kamituga Rift, respectively.

The analysis of the length distribution of active faults yields information on the phase of rift maturity of the Luama and Kamituga Rifts. For the Luama Rift, strain is localized in the inward-dipping SW faults, including the Kataki Fault, resulting in a predominant power-law distribution result; these results indicate that the Luama Rift is in the border-faulted stage of rift phase maturity. For the Kamituga Rift, we interpret the power-law distribution result and the polarity in the dominant fault dips as an incipient stage of rifting. Overall, these results suggest that the Kamituga Rift is on the verge of entering its border-faulting stage. A closer examination of the rift reveals that the northern Kamituga basin has established a border fault, the Kasika Fault, but the southern Kamituga basin is dominated by the Kisengela and Mizinga synthetic Faults with similar length and offset, indicating no border fault in that section of the rift. The Kisengela and Mizinga Faults could be considered the border fault if merged at the surface, similar to the Bilila-Mtakataka and Chirobwe-Ncheu Faults in the S. Malawi Rift, where both faults define border fault splays (Kolawole, Firkins, et al., 2021; Ojo et al., 2022). Thus, although the northern Kamituga basin hosts the Kasika border Fault, the rift as a whole is not border-faulted. Furthermore, the Luama Rift fault lengths are generally longer than the Kamituga Rift fault lengths, indicating that more fault growth and strain accommodation have occurred in the Luama Rift. Due to the asymptotically long-scale approximation of time-space fault evolution (Spyropoulos et al., 2002), we infer that the reactivated rifts will continue to exhibit the same fault length distribution before rift failure, and the fault length distribution will evolve as expected, regardless of the length of inactivity periods.

5.2. Rift Initiation in Cold Continental Lithosphere

5.2.1. Regional Stress Field

Our slip tendency analysis indicates that the active faults in the Luama and Kamituga Rifts are optimally oriented for failure in the EARS stress field, with a 0.55 fault rock friction coefficient and a cohesion of less than 20 MPa. In the Luama Rift, NW–SE striking and SW-dipping active faults exhibit the highest slip tendency to the adjacent North Tanganyika stress field. Many of the other faults (inferred inactive faults) trend parallel to the active faults with high slip tendency, suggesting that they may have started to reactivate but have lower slip rates. Some may be in the strain shadow of larger faults, resulting in erosion rates that outpace their slip rates. In the Kamituga Rift, the mapped faults exhibit the highest slip tendency in relation to the adjacent Kivu stress field. The dominant dip in the faults located in the northern Kamituga basin is NW, suggesting compatibility with the adjacent Kivu Rift

stress field. In contrast, the southern basin is predominantly SE. This change in dip direction suggests a slight rotation in the tectonic stress from the northern Kamituga sub-basin to the southern sub-basin.

Overall, the reactivated faults in the Luama and Kamituga Rifts are consistent with the contemporary stress field of the EARS, suggesting that stresses from the active plate boundary are reactivating these faults. Inherited weaknesses in the basement, most prominently the polyphase orogenesis intersection area between the Paleoproterozoic NW-trending Ruzizian-Ubendian Belt, the Mesoproterozoic NW-trending Kibaran Belt, and the Mesoproterozoic heavily folded Karagwe-Ankole Belt, along with pre-rift structures, including Karoo faults, and the evolution of the stress field orientation, had a significant influence on rift evolution and probably controls rift reactivation (Holdsworth et al., 1997).

5.2.2. The Roles of Melt and Inherited Lithospheric Boundaries

We explore the recently published full-waveform inversion seismic tomographic velocity model of the lithospheric mantle beneath East Africa (van Herwaarden et al., 2023) for other possible sources of tectonic stress perturbation. The shear wave speed model shows that there is a low-velocity anomaly in the mantle lithosphere beneath the Kivu Rift that extends beneath the Kamituga Rift and is collocated with the Quaternary Bukavu and Mwegna-Kamituga volcanic provinces (Figure 9). The lithosphere-aesthenosphere boundary (LAB) depth is estimated by converting the shear wave speed from the tomographic model into temperatures (Ajala et al., 2025; Ajala & Kolawole, 2024). To calculate the LAB depth, a steady-state geotherm is fitted to the shear wave speed-derived temperature profile below 40 km, based on surface heat flow between 30 and 90 mW/m^2, to account for uncertainties at lower temperatures. The LAB is then defined where the conductive and convective geotherms intersect, assuming a mantle potential temperature of 1,300°C. The LAB depth estimated from the model rapidly deepens beneath the southern Kamituga Rift (Figure 9b; Ajala & Kolawole, 2024). The LAB depths from Priestley et al. (2024) show a similar pattern (see Figure S4 in Supporting Information S1 for a comparison with earlier available LAB models). We interpret the low shear wave speed anomaly as a geophysical signature of elevated mantle temperatures and the presence of partial melts in the thinned lithospheric mantle beneath the Kamituga Rift. The Mwegna-Kamituga volcanic field lacks caldera volcanic edifices, indicating that diking is likely the primary mechanism of magma-plumbing and surface eruption (i.e., fissure eruption). Thus, we argue that lithospheric thinning and tectonic extension in the Kamituga Rift is hybrid: the northern sub-basin is magma-assisted, and the southern sub-basin is fault-controlled. A similar hybrid rifting model has been previously suggested for the Kivu Rift (Wauthier et al., 2015). We also argue that early lithospheric necking is the dominant mechanism of lithospheric weakening and regional stress perturbation in the Kamituga Rift segment of the rift zone.

Our observations of low velocity and thinned lithosphere beneath the Kamituga Rift supports that lithospheric warming via melt emplacements in the crust and upper mantle facilitated rift initiation at the location, southwestwards of the Kivu Rift. However, the relatively colder lithosphere beneath the reactivating Luama Rift (Figure 9c) raises a question on the mechanism for lithospheric weakening to observe the persistent Quaternary fault reactivation along the rift. We propose that the Kibaran-Ruzizian suture in the Luama Rift represents a long-lived lithospheric-scale zone of mechanical weakness in the rift zone that might be localizing the regional tectonic strain (Figures 10a, 10c and 11). We note that the low shear wave speed anomalies observed in the Kamituga and Kivu Rifts do not extend into the Tanganyika Rift or the Luama Rift (Figures 9c and 9d), probably due to limited tomographic resolution or low melt volume in those areas.

5.3. Nucleation of the Itombwe Microplate: A Previously Unknown Microplate of the EARS

The reactivated Luama and Kamituga Rifts, along with the adjacent Tanganyika and Kivu Rifts, reveal the axes of rifting in this part of the EARS' western branch. Considering the incipient nature of rifting in the Luama and Kamituga Rifts, we propose these less-studied rifts to be active segments of the EARS Western Branch west of the previously proposed axes of extension in the region (Figure 10a). The previously proposed axis goes through the Kivu Rift and continues southward through the Tanganyika Rift. Our revision of the rift axes kinks westward through the Kamituga Rift southwest of the Kivu Rift and again, kinks southeastward through the Luama Rift, to eventually rejoin the central Tanganyika Rift. These results imply that the EARS Western Branch axis bifurcates south of the Kivu Rift, maintaining two active rift axes: a western axis through the Luama-Kamituga Rifts and an eastern axis through the Kivu-Tanganyika Rifts.

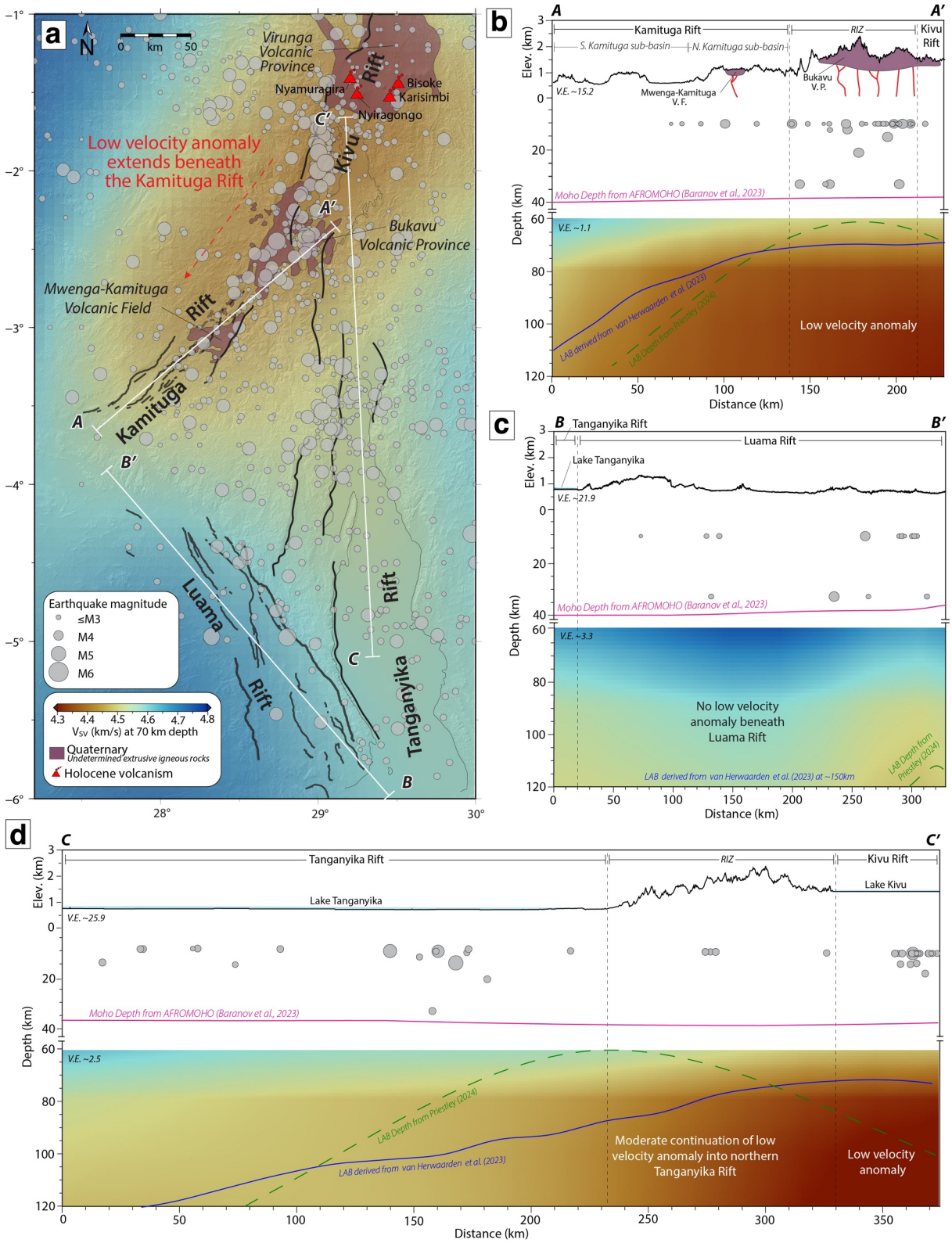

Figure 9. (a) Shuttle Radar Topography Mission-Digital Elevation Model hillshade map overlain by SV wave speeds at 70 km depth from the seismic tomography model of van Herwaarden et al. (2023). (b–d) S wave speeds along profiles A–A′, B–B′, and C–C′, highlighted in panel a. The blue line represents the lithosphere-asthenosphere boundary (LAB) derived from the model of van Herwaarden et al. (2023) (Ajala & Kolawole, 2024), the green dashed line is the LAB obtained from Priestley et al. (2024), and the pink solid line is the Moho depth from Baranov et al. (2023).

10.1029/2025TC008815

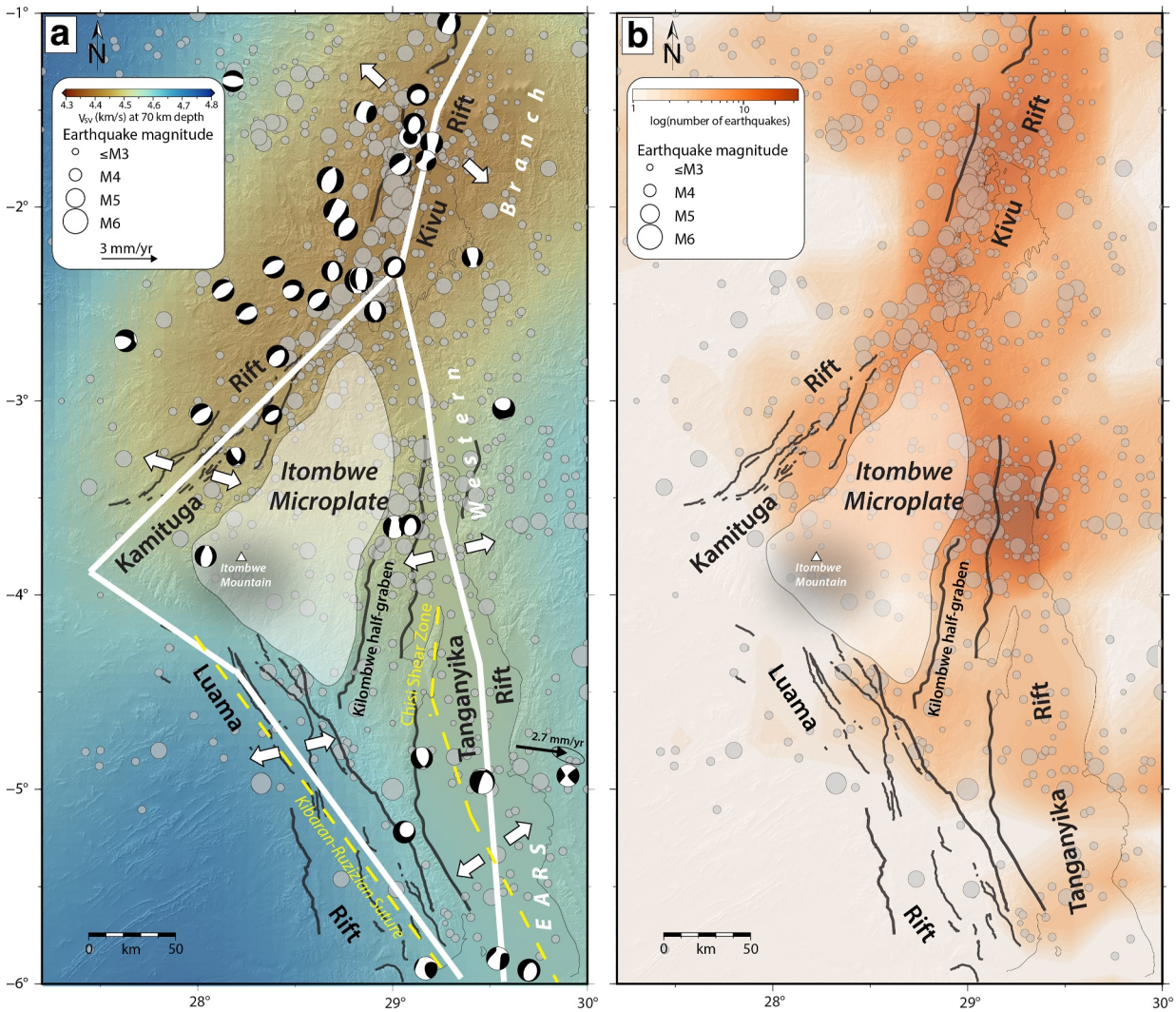

Figure 10. The Itombwe Microplate and wider EARS rifting axes. (a) Shuttle Radar Topography Mission-Digital Elevation Model hillshade overlain with shear wave speed at 70 km depth, earthquakes, moment tensors, and local stress fields. The map shows our proposed revision of the EARS Western Branch, which includes a wider zone of extension characterized by the broader region of seismicity extending westward from the previously known EARS axis (i.e., Kivu-Tanganyika-Rukwa axis). (b) Contoured earthquake density map gridded 0.25° × 0.25° and linearly interpolated.

The activation of the Luama and Kamituga Rifts, together with the Tanganyika Rift, delineates the nucleation of a microplate, hereinafter named "Itombwe Microplate" (after the Massif D'Itombwe; Figure 10). The southeastern margin of the microplate is bounded by the Kilombwe Fault and half-graben (Figures 6g, 10a, and 10b) where active rift subsidence is evidenced by the Kilombwe Marsh and active fault scarps on-shore and west of Lake Tanganyika. We define the Itombwe Microplate as a ∼10,000 km^2 (∼80-km wide, ∼125-km long) tectonic block that is evolving along the segments of the magma-poor Western Branch of the EARS. We interpret the Itombwe Microplate following the concept of Plate Tectonic Theory: a relatively small-scale, rigid, geological block with a consistent motion in present-day space bounded by active (divergent) plate boundaries (i.e., the "micro-block" of Li et al. (2018)). In regions of active non-volcanic tectonic extension, the plate boundary axes are often inferred and defined from the spatial distribution of earthquake data collocated with Holocene fault scarps (e.g., Grant et al., 2024; Mulibo & Nyblade, 2016). However, seismicity in the Luama-Kamituga Rift Zone is more concentrated within the rifts and diffuse across the microplate (Figure 10b). Previous studies have found that incipient oceanic microplates do not necessarily behave rigidly and often experience pervasive internal deformation before becoming more rigid at the later stages of development (Bird et al., 1998). The earthquake density map of the Luama-Kamituga Rift Zone (Figure 10b) highlights the presence of seismicity across the northern

10.1029/2025TC008815

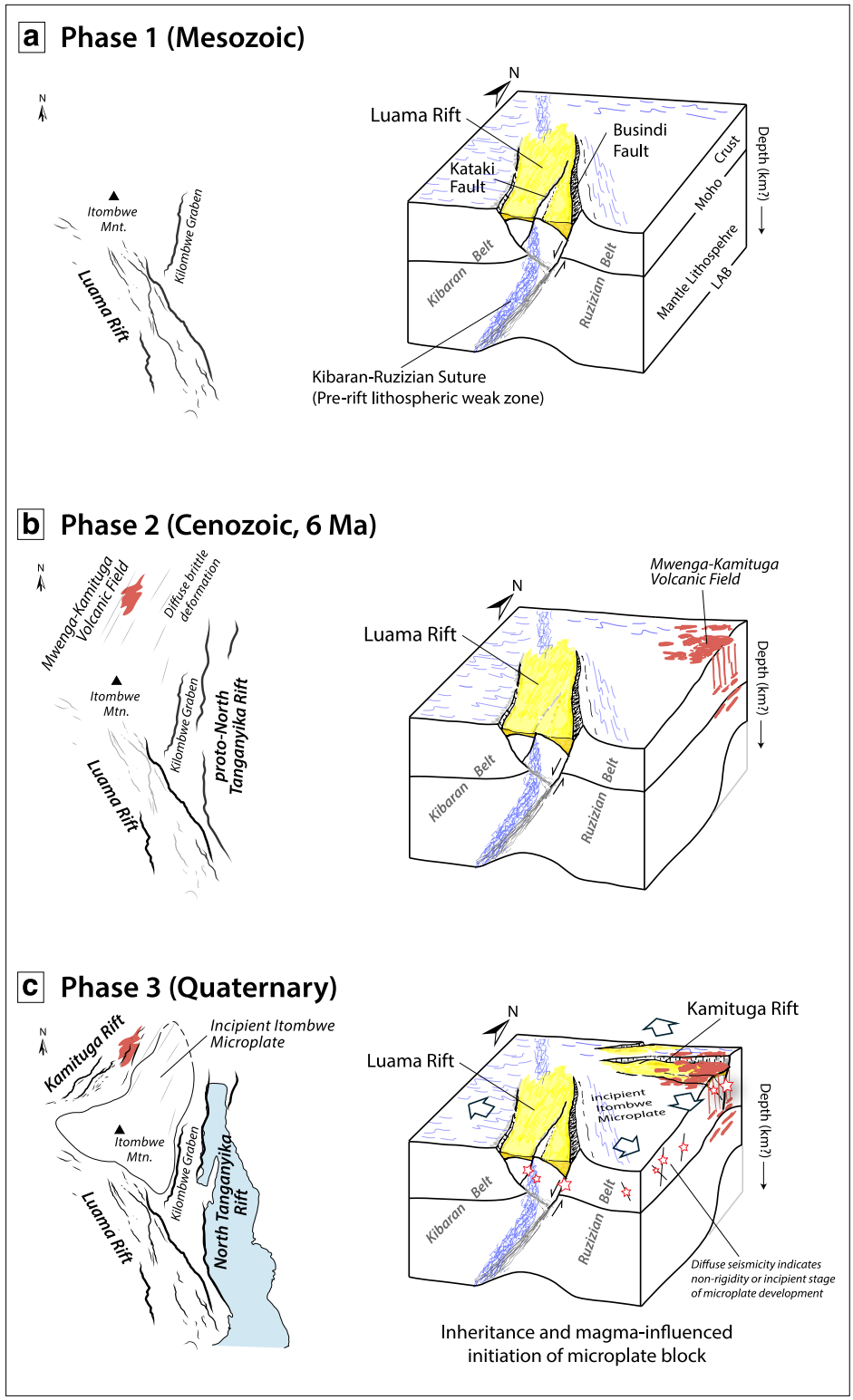

Figure 11. Schematic block diagram summarizing the three main tectonic phases of the Luama-Kamituga Rift Zone. (a) The initiation of the Luama Rift during the Mesozoic (Phase 1). (b) Fissure eruptions in the Mwenga-Kamituga Volcanic Field starting in the Cenozoic, 6 Ma, as dated by Kampunzu et al. (1998). The Luama Rift is inactive, a remnant "failed" Mesozoic Rift. Diffuse brittle deformation is also occurring in the area north of the Luama Rift. (c) Reactivation of the Luama and Kamituga Rifts and nucleation of the Itombwe Microplate. The white arrows are direction of tectonic extension. The stars represent earthquakes.

portion of the microplate, suggesting diffuse brittle deformation is occurring in the interior of the Itombwe Microplate. We examined topography hillshade maps of the Itombwe Microplate for surface manifestations of brittle structures and mapped several >15 km-long rectilinear megafractures (Figure S5 in Supporting Information S1). The megafractures are dominantly NNE-striking, parallel to the Kamituga Rift, and thus may have possibly nucleated earlier as regional distributed deformation across the region during the onset of initiation of the Kamituga Rift. These mega-fractures are favorably oriented to the Kamituga Rift tectonic field (Figures 7a–7c and Figure S5 in Supporting Information S1) and might have taken up a small proportion of the early-rift extensional strain. Thus, we propose that the Itombwe microplate is accommodating some internal deformation, indicating either its non-rigidity and/or penetrative deformation in the incipient stages of microplate development.

An important criterion for defining an active microplate is independent and consistent motion, typically confirmed through geodetic studies (e.g., the Victoria Microplate in the EARS, as described in Calais et al., 2006). Here, the lack of GPS stations does not allow the evaluation of the kinematics of the Itombwe Microplate. The microplate may probably be accommodating some rotational strain, and the 2.7 mm/yr geodetic strain rate estimated for Tanganyika Rift (Figure 10a; Saria et al., 2014) is likely an overestimate considering active extension in the Luama and Kamituga Rifts. However, there is currently no information on strain rates for each rift due to the lack of GPS data in the Luama-Kamituga Rift Zone (Figure 10a; Saria et al., 2014). Variations in rift plate stretching rates along the bounding rift zones may induce internal deformation of the microplate and/or apparent rotation of the microplate about a vertical axis. The presence of a strong lithospheric domain along a continental microplate margin has been suggested as a requirement for rotation about a vertical axis of a microplate (Glerum et al., 2020). The Luama and Kamituga Rifts are poorly coalesced and define an orthogonal tip-to-tip rift interaction zone in the Namoya area, thus implying a "strong" intervening lithosphere that may allow for the Itombwe Microplate's rotation. Similarly, if the lithosphere has not yet been significantly weakened beneath the reactivating Luama Rift, it might remain strong, implying a possible rotation of the Itombwe Microplate (Figure 9b).

We consider that the nucleation of the Itombwe Microplate is being facilitated by a "structural template" defined by the reactivating (previously failed) Luama Rift and the inheritance of polyphase orogenic belts with orthogonal fabrics (Figures 1c and 11). Along the western margin of the microplate, specifically the Kamituga Rift, there is likely more magma-influence on tectonic extension than along its eastern and southern margins, given the absence of volcanics in the Luama Rift and the northern Tanganyika Rift. Geodynamic studies have shown that the inheritance of narrow accreted orogenic terranes, bounded by lithospheric-scale suture zones, may nucleate microplates during continental extension (Heron et al., 2023). We propose that the inheritance of the NW-striking Ruzizian-Ubendian suture in the Luama Rift lithosphere, and the presence of a N–S striking strand of the Precambrian Chisi Shear Zone beneath the northern Tanganyika Rift axis (Figure 10a; Kolawole, Phillips, et al., 2021) could have provided an inherited mechanical anisotropy template that aided the nucleation of rifts with oblique/orthogonal axial orientations to initiate the Itombwe microplate.

If continental break-up is successful along the rifts of the EARS, the Victoria, Itombwe, Rovuma, and Lwandle tectonic microplates will form an archipelago of isolated or stranded micro-continents, a phenomenon observed worldwide (Irwin, 1972; Vink et al., 1984). Notable examples include Gondwana's fossil microplates now found in New Zealand and Madagascar (Mortimer, 2004; Stern, 1994). Over geological time, these stranded microplates might collide, amalgamate, and form new continents. One example is Avalonia, a Paleozoic microplate that developed on the margin of Rodinia, rifted off and became a drifting microplate, and eventually accreted onto the Baltica continent (e.g., Servais & Sintubin, 2009). The delineation of the Itombwe Microplate raises new and exciting science questions on incipient microplates and how they respond to strain partition across their bounding rift segments in the presence of localized magmatism.

6. Conclusions

We integrated SRTM-DEM, distribution of surface displacements, rift morphology, Mohr-Coulomb slip tendency analysis, and fault length scaling to investigate first-order controls on microplate geometry during plate boundary initiation. We focus on two contiguous poorly studied rift basins, the NW-trending Luama Rift and NE-trending Kamituga Rift in the EARS Western Branch, where the Paleoproterozoic NW-trending Ruzizian-

Ubendian, the Mesoproterozoic NE-trending Kibaran and Karagwe-Ankole, and the Neoproterozoic Itombwe Belt overlap in a polyphase orogenic intersection zone. Our results show that:

1. The Luama and Kamituga Rifts are undergoing early-stage lithospheric extension, driven by the tectonic forces of the East African Rift System (EARS).
2. Brittle reactivation of the Ruzizian-Ubendian suture, along with other exhumed Precambrian shear zones, accommodated rift initiation along the Kamituga and Luama Rifts, and may be playing an essential role in the modern reactivation of the rift zone.
3. Overall, the Luama-Kamituga Rift Zone marks the continuation of the EARS, delineating the nucleation of a new microplate, hereinafter referred to as the "Itombwe Microplate." The continuation of the delineated active rift axes into the eastern Democratic Republic of Congo indicates that the zone of strain accommodation along the Western Rift of the East African Rift System is significantly wider than previously thought.
4. Reactivation of failed rifts, Precambrian suture zones, and inheritance of polyphase orogenic belts with orthogonal fabrics created a structural template for the development of Itombwe Microplate.
5. Diffuse seismicity across the microplate either indicates its non-rigidity or incipient phase of development.

Conflict of Interest

The authors declare no conflicts of interest relevant to this study.

Data Availability Statement

The fault database for the Luama and Kamituga Rifts is openly available at Zenodo Data Repository (Colet et al., 2025): https://zenodo.org/records/14605488. The Shuttle Radar Topography Mission data is available through USGS Earth Explorer (https://earthexplorer.usgs.gov; Houska, 2012). The focal mechanisms and stress fields used in this study are compiled in Tables S1 and S2 in Supporting Information S1. The Win-Tensor program is available at http://damiendelvaux.be/Tensor/WinTensor/win-tensor.html (Delvaux, 2012).

Acknowledgments
This project was supported through Grants from the G. Unger Vetlesen Foundation, awarded to F. Kolawole. We thank Derek Keir and an anonymous reviewer for their insightful, thorough, and highly constructive reviews, and Taylor Schildgen for the editorial handling. Figures 1, 4, 9 and 10 were created using the Generic Mapping Tools (GMT) and its Python equivalent, PyGMT (Uieda et al., 2021; Wessel et al., 2019). Figure S5 in Supporting Information S1 was made using GeoMapApp (www.geomapapp.org)/CC BY/CC BY (Ryan et al., 2009).

References

Ajala, R., & Kolawole, F. (2024). Lithosphere-asthenosphere boundary map of the African plate (1.0.0) [Dataset]. *Zenodo*. https://doi.org/10.5281/zenodo.14573774

Ajala, R., Kolawole, F., Legre, J.-J., Olugboji, T., van Herwaarden, D.-P., & Fichtner, A. (2025). Multiscale comparison of early-stage lithospheric deformation styles in magma-poor and magma-rich divergent plate boundaries. *EES Open Archive*. https://doi.org/10.22541/au.173627299.94095848/v1

Ajala, R., Kolawole, F., & Manke, W. (2024). Blind magmatism abets nonvolcanic continental rifting. *Communications Earth & Environment*, *5*(1), 80. https://doi.org/10.1038/s43247-024-01244-7

Angelier, J. (1989). From orientation to magnitudes in Paleostress determinations using fault slip data. *Journal of Structural Geology*, *11*(1), 37–50. https://doi.org/10.1016/0191-8141(89)90034-5

Angelier, J., & Mechler, P. (1977). Sur une methode graphique de recherche des contraintes principales egalement utilisables en tectonique et en seismologie: La methode des diedres droits. *Bulletin de la Societe Geologique de France*, *S7-XIX*(6), 1309–1318. https://doi.org/10.2113/gssgfbull.S7-XIX.6.1309

Avouac, J.-P. (1993). Analysis of scarp profiles: Evaluation of errors in morphologic dating. *Journal of Geophysical Research*, *98*(B4), 6745–6754. https://doi.org/10.1029/92JB01962

Baranov, A., Tenzer, R., Eitel, F., & Ghmosi, K. (2023). A new Moho map of the African continent from seismic, topographic, and tectonic data. *Gondwana Research*, *124*, 218–245. https://doi.org/10.1016/j.gr.2023.06.019

Bendat, J. S., & Piersol, A. G. (2011). *Random data: Analysis and measurement procedures*. John Wiley & Sons.

Bernacsek, G. M., Hughes, J. S., & Hughes, R. H. (1992). *A directory of African wetlands*. IUCN. Retrieved from https://portals.iucn.org/library/node/6001

Bird, R. T., Naar, D. F., Larson, R. L., Searle, R. C., & Scotese, C. R. (1998). Plate tectonic reconstructions of the Juan Fernandez microplate: Transformation from internal shear to rigid rotation. *Journal of Geophysical Research*, *103*(B4), 7049–7067. https://doi.org/10.1029/97jb02133

Boniface, N., & Schenk, V. (2012). Neoproterozoic eclogites in the paleoproterozoic Ubendian belt of Tanzania: Evidence for a pan-African suture between the Bangweulu block and the Tanzania craton. *Precambrian Research*, *208–211*, 72–89. https://doi.org/10.1016/j.precamres.2012.03.014

Boniface, N., Schenk, V., & Appel, P. (2012). Paleoproterozoic eclogites of MORB-type chemistry and three Proterozoic orogenic cycles in the Ubendian Belt (Tanzania): Evidence from monazite and zircon geochronology, and geochemistry. *Precambrian Research*, *192–195*, 16–33. https://doi.org/10.1016/j.precamres.2011.10.007

Boniface, N., & Tsujimori, T. (2021). New tectonic model and division of the Ubendian-Usagaran Belt, Tanzania: A review and in-situ dating of eclogites. In J. Wakabayashi, Y. Dilek, & J. Wakabayashi (Eds.), *Plate tectonics, ophiolites, and societal significance of geology: A celebration of the career of Eldridge Moores* (Vol. 552). Geological Society of America. https://doi.org/10.1130/2021.2552(08)

Boven, A., Theunissen, K., Sklyarov, E., Klerkx, J., Alexander, M., Mruma, A., & Punzalan, L. (1999). Timing of exhumation of a high-pressure mafic granulite terrane of the Paleoproterozoic Ubende belt (West Tanzania). *Precambrian Research*, *93*(1), 119–137. https://doi.org/10.1016/S0301-9268(98)00101-6

Brown, S. R., & Scholz, C. H. (1985). Broad bandwidth study of the topography of natural rock surfaces. *Journal of Geophysical Research*, *90*(B14), 12575–12582. https://doi.org/10.1029/JB090iB14p12575

Brune, S., Kolawole, F., Olive, J.-A., Stamps, D. S., Buck, W. R., Buiter, S. J. H., et al. (2023). Geodynamics of continental rift initiation and evolution. *Nature Reviews Earth & Environment*, *4*(4), 235–253. https://doi.org/10.1038/s43017-023-00391-3

Burbank, D. W., & Anderson, R. S. (2013). Tectonic geomorphology, second edition. *Environmental and Engineering Geoscience*, *19*(2), 198–200. https://doi.org/10.2113/gseegeosci.19.2.198

Cahen, L. (1952). Les groupes de l'Urundi, du Kibali et de la Rusizi au Congo oriental et nord-oriental. *Annales de la Société Géologique de Belgique*, *75*, 1–64.

Cahen, L. (1954). *Géologie du Congo belge*. H. Vaillant-Carmanne. 577.

Cahen, L., Ledent, D., & Villeneuve, M. (1979). Existence d'une chaîne plissée Protérozoïque supérieur au Kivu oriental (Zaïre). Données géochronologiques relatives au Supergroupe de l'Itombwe. *Bulletin de la Societe Belge de Geologie*, *88*(1–2), 71–83.

Calais, E., Ebinger, C., Hartnady, C., & Nocquet, J. M. (2006). Kinematics of the East African Rift from GPS and earthquake slip vector data. *Geological Society of London*, *259*(1), 9–22. https://doi.org/10.1144/gsl.sp.2006.259.01.03

Castaing, C. (1991). Post-Pan-African tectonic evolution of South Malawi in relation to the Karroo and recent East African rift systems. *Tectonophysics*, *191*(1–2), 55–73. https://doi.org/10.1016/0040-1951(91)90232-h

Choubert, G., & Faure-Muret, A. (1987). *Carte géologique internationale de l'Afrique, 1/5 000 000*. Carte géologique internationale de l'Afrique, 1/5 000 000. Paris: CCGM.

Clauset, A., Shalizi, C. R., & Newman, M. E. J. (2009). Power-law distributions in empirical data. *SIAM Review*, *51*(4), 661–703. https://doi.org/10.1137/070710111

Colet, M., Kolawole, F., Ajala, R., Delvaux, D., & Nkodia, H. M. D.-V. (2025). Luama and Kamituga rifts fault database (1.0.0) [Dataset]. *Zenodo*. https://doi.org/10.5281/zenodo.14605488

Corti, G., Maestrelli, D., & Sani, F. (2022). Large-to local-scale control of pre-existing structures on continental rifting: Examples from the main Ethiopian rift, East Africa. *Frontiers in Earth Science*, *10*. https://doi.org/10.3389/feart.2022.808503

Corti, G., van Wijk, J., Cloetingh, S., & Morley, C. K. (2007). Tectonic inheritance and continental rift architecture: Numerical and analogue models of the East African Rift system. *Tectonics*, *26*(6). https://doi.org/10.1029/2006TC002086

Cowie, P. A., Sornette, D., & Vanneste, C. (1995). Multifractal scaling properties of a growing fault population. *Geophysical Journal International*, *122*(2), 457–469. https://doi.org/10.1111/j.1365-246X.1995.tb07007.x

Cowie, P. A., Underhill, J. R., Behn, M. D., Lin, J., & Gill, C. E. (2005). Spatio-temporal evolution of strain accumulation derived from multi-scale observations of late Jurassic rifting in the northern North sea: A critical test of models for lithospheric extension. *Earth and Planetary Science Letters*, *234*(3), 401–419. https://doi.org/10.1016/j.epsl.2005.01.039

Daly, M. C. (1988). Crustal shear zones in central Africa: A kinematic approach to proterozoic tectonics. *International Union of Geological Sciences*, *11*(1), 5–11. https://doi.org/10.18814/epiiugs/1988/v11i1/003

Daly, M. C., Chorowicz, J., & Fairhead, J. D. (1989). Rift basin evolution in Africa: The influence of reactivated steep basement shear zones. *Geological Society, London, Special Publications*, *44*(1), 309–334. https://doi.org/10.1144/GSL.SP.1989.044.01.17

De Bie, S. (2015). *Petrographical, mineralogical and geochemical study of the Au mineralisation at Namoya, Maniema (DRC)* (Master of Science thesis). KU Leuven & Universiteit Gent, supervised by P. Muchez, and co-supervised by S. Dewaele.

Deblond, A., Punzalan, L. E., Boven, A., & Tack, L. (2001). The Malagarazi supergroup of southeast Burundi and its correlative Bukoba supergroup of northwest Tanzania: Neo- and mesoproterozoic chronostratigraphic constraints from Ar–Ar ages on mafic intrusive rocks. *Journal of African Earth Sciences*, *32*(3), 435–449. https://doi.org/10.1016/S0899-5362(01)90107-1

Debruyne, D., Hulsbosch, N., Van Wilderode, J., Balcaen, L., Vanhaecke, F., & Muchez, P. (2015). Regional geodynamic context for the mesoproterozoic Kibara Belt (KIB) and the Karagwe-Ankole belt: Evidence from geochemistry and isotopes in the KIB. *Precambrian Research*, *264*, 82–97. https://doi.org/10.1016/j.precamres.2015.04.001

Delvaux, D. (1989). The Karoo to recent rifting in the western branch of the East-African Rift System: A bibliographical synthesis. Roy Museum. *Afr. Central Tervuren (Department of Geology. Min., Rap. Ann.)*, *1990*, 63–83.

Delvaux, D. (2001). *Karoo rifting in western Tanzania: Precursor of Gondwana break-up? Contributions to geology and paleontology of Gondwana in honor of Helmut Wopfner, geological Institute* (pp. 111–125). University of Cologne.

Delvaux, D. (2011). Win-Tensor, an interactive computer program for fracture analysis and crustal stress reconstruction.

Delvaux, D. (2012). Release of program win-Tensor 4.0 for tectonic stress inversion: Statistical expression of stress Parameters.

Delvaux, D., & Barth, A. (2010). African stress pattern from formal inversion of focal mechanism data. *Tectonophysics*, *482*(1), 105–128. https://doi.org/10.1016/j.tecto.2009.05.009

Delvaux, D., Ganza, G. B., Fiama, S. B., & Havenith, H.-B. (2022). Architecture and evolution of the Kivu Rift within the western branch of the East African Rift System: Implications for seismic hazard assessment. In M. Meghraoui, N. Sundararajan, S. Banerjee, K.-G. Hinzen, M. Eshagh, F. Roure, et al. (Eds.), *Advances in geophysics, tectonics and petroleum geosciences* (pp. 37–40). Springer International Publishing. https://doi.org/10.1007/978-3-030-73026-0_10

Delvaux, D., Mulumba, J.-L., Sebagenzi, M. N. S., Bondo, S. F., Kervyn, F., & Havenith, H.-B. (2017). Seismic hazard assessment of the Kivu rift segment based on a new seismotectonic zonation model (western branch, East African Rift system). *Journal of African Earth Sciences*, *134*, 831–855. https://doi.org/10.1016/j.jafrearsci.2016.10.004

Delvaux, D., & Sperner, B. (2003). New aspects of tectonic stress inversion with reference to the TENSOR program. *Geological Society, London, Special Publications*, *212*(1), 75–100. https://doi.org/10.1144/GSL.SP.2003.212.01.06

Dunn, S. C., & von der Heyden, B. P. (2022). Proterozoic – Paleozoic orogenic gold mineralization along the southwestern margin of the Tanzania craton: A review. *Journal of African Earth Sciences*, *185*, 104400. https://doi.org/10.1016/j.jafrearsci.2021.104400

Ekström, G., Nettles, M., & Dziewonski, A. M. (2012). The global CMT project 2004–2010: Centroid-moment tensors for 13,017 earthquakes. *Physics of the Earth and Planetary Interiors*, *200–201*, 1–9. https://doi.org/10.1016/j.pepi.2012.04.002

Evans, D. M., Barrett, F. M., Prichard, H. M., & Fisher, P. C. (2012). Platinum–palladium–gold mineralization in the Nkenja mafic–ultramafic body, Ubendian metamorphic belt, Tanzania. *Mineralium Deposita*, *47*(1), 175–196. https://doi.org/10.1007/s00126-011-0353-8

Fernandez-Alonso, M., Cutten, H., De Waele, B., Tack, L., Tahon, A., Baudet, D., & Barritt, S. D. (2012). The Mesoproterozoic Karagwe-Ankole Belt (formerly the NE Kibara Belt): The result of prolonged extensional intracratonic basin development punctuated by two short-lived far-field compressional events. *Precambrian Research*, *216–219*, 63–86. https://doi.org/10.1016/j.precamres.2012.06.007

Fernandez-Alonso, M., & Theunissen, K. (1998). Airborne geophysics and geochemistry provide new insights in the intracontinental evolution of the Mesoproterozoic Kibaran belt (Central Africa). *Geological Magazine*, *135*(2), 203–216. https://doi.org/10.1017/s0016756898008310

Ferrill, D. A., Morris, A. P., Jones, S. M., & Stamatakos, J. A. (1998). Extensional layer-parallel shear and normal faulting. *Journal of Structural Geology*, *20*(4), 355–362. https://doi.org/10.1016/S0191-8141(97)00090-4

Frohlich, C. (1992). Triangle diagrams: Ternary graphs to display similarity and diversity of earthquake focal mechanisms. *Physics of the Earth and Planetary Interiors*, *75*(1), 193–198. https://doi.org/10.1016/0031-9201(92)90130-N

Ganbat, A., Tsujimori, T., Boniface, N., Pastor-Galán, D., Aoki, S., & Aoki, K. (2021). Crustal evolution of the paleoproterozoic ubendian belt (SW Tanzania) western margin: A central African Shield amalgamation tale. *Gondwana Research*, *91*, 286–306. https://doi.org/10.1016/j.gr.2020.12.009

Gawthorpe, R. L., & Leeder, M. R. (2000). Tectono-sedimentary evolution of active extensional basins. *Basin Research*, *12*(3–4), 195–218. https://doi.org/10.1111/j.1365-2117.2000.00121.x

Glerum, A., Brune, S., Stamps, D. S., & Strecker, M. R. (2020). Victoria continental microplate dynamics controlled by the lithospheric strength distribution of the East African Rift. *Nature Communications*, *11*(1), 2881. https://doi.org/10.1038/s41467-020-16176-x

Gloire, A. B., Lucien, M. M., Gloire, G. B., & Robert, N. W. (2022). Petrographic and kinematic analysis of the Itombwe synclinorium formations exposed at Tshondo and Bugoy (South-Kivu region, Democratic Republic of the Congo). *Environmental & Earth Sciences Research Journal*, *9*(3), 104–113. https://doi.org/10.18280/eesrj.090304

Gouiza, M., & Naliboff, J. (2021). Rheological inheritance controls the formation of segmented rifted margins in cratonic lithosphere. *Nature Communications*, *12*(1), 4653. https://doi.org/10.1038/s41467-021-24945-5

Grant, C., Kolawole, F., & Williams, J. (2024). Evolution of rift faulting in incipient, magma-poor divergent plate boundaries: New insights from the Okavango-Makgadikgadi Rift Zone, Botswana. *Earth and Planetary Science Letters*, *646*, 118957. https://doi.org/10.1016/j.epsl.2024.118957

Gupta, A., & Scholz, C. H. (2000). Brittle strain regime transition in the Afar depression: Implications for fault growth and seafloor spreading. *Geology*, *28*(12), 1087–1090. https://doi.org/10.1130/0091-7613(2000)28<1087:BSRTIT>2.0.CO;2

Heron, P. J., Peace, A. L., McCaffrey, K. J. W., Sharif, A., Yu, A. J., & Pysklywec, R. N. (2023). Stranding continental crustal fragments during continent breakup: Mantle suture reactivation in the Nain Province of Eastern Canada. *Geology*, *51*(4), 362–365. https://doi.org/10.1130/G50734.1

Holdsworth, R., Butler, C., & Roberts, A. (1997). The recognition of reactivation during continental deformation. *Journal of the Geological Society*, *154*(1), 73–78. https://doi.org/10.1144/gsjgs.154.1.0073

Houska, T. (2012). *EarthExplorer*. General Information Product. https://doi.org/10.3133/gip136

Ilombe, G. M., Mukokya, Y. M., Nzolang, C., Kalikone, C. B., Birhenjira, E. M., Mugaruka, B. T., & Delvaux, D. (2017). Geology and structure of Mobale gold deposit at Kamituga: A contribution to the study of the Kivu supergroup. *Geo-Eco-Trop*, *41*(2), 151–168.

Irwin, W. P. (1972). *Terranes of the western Paleozoic and Triassic belt in the southern Klamath Mountains* (pp. 103–111). Geological Survey Research, Chapter C: U.S. Geological Survey Professional Paper 800-C. https://doi.org/10.3133/pp800C

Jackson, C. A. L., Gawthorpe, R. L., Carr, I. D., & Sharp, I. R. (2005). Normal faulting as a control on the stratigraphic development of shallow marine SYN-rift sequences: The Nukhul and lower Rudeis formations, Hammam Faraun fault block, Suez rift, Egypt. *Sedimentology*, *52*(2), 313–338. https://doi.org/10.1111/j.1365-3091.2005.00699.x

Kampunzu, A., Rumvegeri, B., Kapenda, D., Lubala, R., & Caron, J. (1986). Les Kibarides d'Afrique centrale et orientale: Une chaîne de collision. *United Nations Educational, Scientific, and Cultural Organization, Geological Service for Economic Development Bulletin*, *5*, 125–137.

Kampunzu, A. B., Bonhomme, M. G., & Kanika, M. (1998). Geochronology of volcanic rocks and evolution of the Cenozoic western branch of the East African Rift System. *Journal of African Earth Sciences*, *26*(3), 441–461. https://doi.org/10.1016/S0899-5362(98)00025-6

Kazimoto, E. O., Schenk, V., & Appel, P. (2014). The age of Au–Cu–Pb-bearing veins in the poly-orogenic Ubendian belt (Tanzania): U–Th–total Pb dating of hydrothermally altered monazite. *Contributions to Mineralogy and Petrology*, *169*(1), 1088. https://doi.org/10.1007/s00410-014-1088-1

Kirkpatrick, J. D., Bezerra, F. H. R., Shipton, Z. K., Do Nascimento, A. F., Pytharouli, S. I., Lunn, R. J., & Soden, A. M. (2013). Scale-dependent influence of pre-existing basement shear zones on rift faulting: A case study from NE Brazil. *Journal of the Geological Society*, *170*(2), 237–247. https://doi.org/10.1144/jgs2012-043

Klerkx, J., Lavreau, J., Liégeois, J.-P., & Theunissen, K. (1984). Granitoïdes kibariens précoces et tectonique tangentielle au Burundi: Magmatisme biomodal lié à une distension crustale. In *Géologie africaine* (pp. 29–46).

Klerkx, J., Liégeois, J.-P., Lavreau, J., & Claessens, W. (1987). Crustal evolution of the northern Kibaran belt, eastern and central Africa. *Proterozic Lithospheric Evolution*, *17*, 217–233. https://doi.org/10.1029/gd017p0217

Kokonyangi, J., Armstrong, R., Kampunzu, A. B., Yoshida, M., & Okudaira, T. (2004). U–Pb zircon geochronology and petrology of granitoids from Mitwaba (Katanga, Congo): Implications for the evolution of the mesoproterozoic Kibaran belt. *Precambrian Research*, *132*(1), 79–106. https://doi.org/10.1016/j.precamres.2004.02.007

Kokonyangi, J., Kampunzu, A. B., Poujol, M., Okudaira, T., Yoshida, M., & Shabeer, K. P. (2005). Petrology and geochronology of mesoproterozoic mafic–intermediate plutonic rocks from Mitwaba (D. R. Congo): Implications for the evolution of the Kibaran belt in central Africa. *Geological Magazine*, *142*(1), 109–130. https://doi.org/10.1017/S0016756804009951

Kokonyangi, J. W., Kampunzu, A. B., Armstrong, R., Yoshida, M., Okudaira, T., Arima, M., & Ngulube, D. A. (2006). The mesoproterozoic Kibaride belt (Katanga, SE D.R. Congo). *Journal of African Earth Sciences*, *46*(1), 1–35. https://doi.org/10.1016/j.jafrearsci.2006.01.017

Kolawole, F., Atekwana, E. A., Laó-Dávila, D. A., Abdelsalam, M. G., Chindandali, P. R., Salima, J., & Kalindekafe, L. (2018). Active deformation of Malawi Rift's north basin Hinge zone modulated by reactivation of preexisting Precambrian shear zone fabric. *Tectonics*, *37*(3), 683–704. https://doi.org/10.1002/2017TC004628

Kolawole, F., Firkins, M. C., Al Wahaibi, T. S., Atekwana, E. A., & Soreghan, M. J. (2021). Rift interaction zones and the stages of rift linkage in active segmented continental rift systems. *Basin Research*, *33*(6), 2984–3020. https://doi.org/10.1111/bre.12592

Kolawole, F., Phillips, T. B., Atekwana, E. A., & Jackson, C. A.-L. (2021). Structural inheritance controls strain distribution during early continental rifting, Rukwa Rift. *Frontiers in Earth Science*, *9*, 707869. https://doi.org/10.3389/feart.2021.707869

Kolawole, F., Vick, T., Atekwana, E. A., Laó-Dávila, D. A., Costa, A. G., & Carpenter, B. M. (2022). Strain localization and migration during the pulsed lateral propagation of the Shire Rift Zone, East Africa. *Tectonophysics*, *839*, 229499. https://doi.org/10.1016/j.tecto.2022.229499

Kröner, A. (1977). Non-synchroneity of late Precambrian Glaciations in Africa. *The Journal of Geology*, *85*(3), 289–300. https://doi.org/10.1086/628300

Laghmouch, M., Kalikone, C., Ilombe, G., Ganza, G., Safari, E., Bachinyaga, J., et al. (2018). *Carté Géologique du Kivu, 1/500.000*. Université Officielle de Bukavu et Museé Royal de l'Afrique Centrale.

Laó-Dávila, D. A., Al-Salmi, H. S., Abdelsalam, M. G., & Atekwana, E. A. (2015). Hierarchical segmentation of the Malawi Rift: The influence of inherited lithospheric heterogeneity and kinematics in the evolution of continental rifts. *Tectonics*, *34*(12), 2399–2417. https://doi.org/10.1002/2015TC003953

Lavayssière, A., Drooff, C., Ebinger, C., Gallacher, R., Illsley-Kemp, F., Oliva, S. J., & Keir, D. (2019). Depth extent and kinematics of faulting in the southern Tanganyika Rift, Africa. *Tectonics*, *38*(3), 842–862. https://doi.org/10.1029/2018TC005379

Lavreau, J. (1985). Le Groupe de la Rusizi (Rusizien du Zaïre, Rwanda et Burundi) à la lumière des connaissances actuelles. *Musée Royal Afrique Centrale, Tervuren (Belgique), Dépt. Géologie Minéralogie, Rapport Annuel 1983 – 1984*, 111–119.

Leger, C., Barth, A., Falk, D., Mruma, A. H., Magigitta, M., Boniface, N., et al. (2015). *Minerogenic map of Tanzania 1:1,500,00: Prepared under the program "sustainable management of mineral Resources" 2013–2014: Project ID: P096302*. Dodoma: Geological Survey of Tanzania (GST).

Lenoir, J. L., Liégeois, J.-P., Theunissen, K., & Klerkx, J. (1994). The palaeoproterozoic Ubendian shear belt in Tanzania: Geochronology and structure. *Journal of African Earth Sciences*, *19*(3), 169–184. https://doi.org/10.1016/0899-5362(94)90059-0

Li, S., Suo, Y., Li, X., Liu, B., Dai, L., Wang, G., et al. (2018). Microplate tectonics: New insights from micro-blocks in the global oceans, continental margins and deep mantle. *Earth-Science Reviews*, *185*, 1029–1064. https://doi.org/10.1016/j.earscirev.2018.09.005

Macgregor, D. (2015). History of the development of the East African Rift System: A series of interpreted maps through time. *Journal of African Earth Sciences*, *101*, 232–252. https://doi.org/10.1016/j.jafrearsci.2014.09.016

Macgregor, D. (2017). History of the development of Permian–Cretaceous rifts in East Africa: A series of interpreted maps through time. *Petroleum Geoscience*, *24*(1), 8–20. https://doi.org/10.1144/petgeo2016-155

Massey, F. J., Jr. (1951). The Kolmogorov-Smirnov test for Goodness of fit. *Journal of the American Statistical Association*, *46*(253), 68–78. https://doi.org/10.1080/01621459.1951.10500769

McConnell, R. (1967). The east African rift system. *Nature*, *215*(5101), 578–581. https://doi.org/10.1038/215578a0

McConnell, R. B. (1972). Geological development of the rift System of eastern Africa. *GSA Bulletin*, *83*(9), 2549–2572. https://doi.org/10.1130/0016-7606(1972)83[2549:GDOTRS]2.0.CO;2

Michas, G., Vallianatos, F., & Sammonds, P. (2015). Statistical mechanics and scaling of fault populations with increasing strain in the Corinth Rift. *Earth and Planetary Science Letters*, *431*, 150–163. https://doi.org/10.1016/j.epsl.2015.09.014

Morley, C. K., Cunningham, S. M., Wescott, W. A., & Harper, R. M. (1999). Geology and geophysics of the Rukwa Rift. In C. K. Morley (Ed.), *AAPG studies in geology: Geoscience of rift systems—Evolution of East Africa* (pp. 91–110). https://doi.org/10.1306/St44623C5

Morris, A., Ferrill, D. A., & Henderson, D. B. (1996). Slip-tendency analysis and fault reactivation. *Geology*, *24*(3), 275–278. https://doi.org/10.1130/0091-7613(1996)024<0275:STAAFR>2.3.CO;2

Mortimer, N. (2004). New Zealand's geological foundations. *Gondwana Research*, *7*(1), 261–272. https://doi.org/10.1016/S1342-937X(05)70324-5

Mulibo, G. D., & Nyblade, A. A. (2016). The seismotectonics of Southeastern Tanzania: Implications for the propagation of the eastern branch of the East African Rift. *Tectonophysics*, *674*, 20–30. https://doi.org/10.1016/j.tecto.2016.02.009

Naliboff, J., & Buiter, S. J. H. (2015). Rift reactivation and migration during multiphase extension. *Earth and Planetary Science Letters*, *421*, 58–67. https://doi.org/10.1016/j.epsl.2015.03.050

Nambaje, C., Williams, I. S., Satish-Kumar, M., & Sajeev, K. (2020). Direct evidence for Archean crust in the western domain of the Karagwe Ankole belt, Rwanda: Implications for Neoarchean to paleoproterozoic crustal evolution. *Precambrian Research*, *350*, 105851. https://doi.org/10.1016/j.precamres.2020.105851

Neuharth, D., Brune, S., Glerum, A., Heine, C., & Welford, J. K. (2021). Formation of continental microplates through rift linkage: Numerical modeling and its application to the Flemish cap and Sao Paulo plateau. *Geochemistry, Geophysics, Geosystems*, *22*(4), e2020GC009615. https://doi.org/10.1029/2020GC009615

Nkodia, H. M. D.-V., Miyouna, T., Kolawole, F., Boudzoumou, F., Loemba, A. P. R., Bazebizonza Tchiguina, N. C., & Delvaux, D. (2022). Seismogenic Fault reactivation in western central Africa: Insights from regional stress analysis. *Geochemistry, Geophysics, Geosystems*, *23*(11), e2022GC010377. https://doi.org/10.1029/2022GC010377

Ojo, O. O., Ohenhen, L. O., Kolawole, F., Johnson, S. G., Chindandali, P. R., Atekwana, E. A., & Laó-Dávila, D. A. (2022). Under-Displaced normal faults: Strain accommodation along an early-stage rift-bounding fault in the Southern Malawi rift. *Frontiers in Earth Science*, *10*. https://doi.org/10.3389/feart.2022.846389

Phillips, T. B., Jackson, C. A.-L., Bell, R. E., Duffy, O. B., & Fossen, H. (2016). Reactivation of intrabasement structures during rifting: A case study from offshore southern Norway. *Journal of Structural Geology*, *91*, 54–73. https://doi.org/10.1016/j.jsg.2016.08.008

Poggi, V., Durrheim, R., Tuluka, G. M., Weatherill, G., Gee, R., Pagani, M., et al. (2017). Assessing seismic hazard of the East African rift: A pilot study from GEM and Africa Array. *Bulletin of Earthquake Engineering*, *15*(11), 4499–4529. https://doi.org/10.1007/s10518-017-0152-4

Priestley, K., Ho, T., Takei, Y., & McKenzie, D. (2024). The thermal and anisotropic structure of the top 300 km of the mantle. *Earth and Planetary Science Letters*, *626*, 118525. https://doi.org/10.1016/j.epsl.2023.118525

Ratcliffe, N. M., Burton, W. C., D'Angelo, R. M., & Costair, J. K. (1986). Low-angle extensional faulting, reactivated mylonites, and seismic reflection geometry of the Newark basin margin in eastern Pennsylvania. *Geology*, *14*(9), 766. https://doi.org/10.1130/0091-7613(1986)14<766:LEFRMA>2.0.CO;2

Ring, U. (1994). The influence of preexisting structure on the evolution of the Cenozoic Malawi rift (East African rift system). *Tectonics*, *13*(2), 313–326. https://doi.org/10.1029/93TC03188

Ring, U. (1995). Tectonic and lithological constraints on the evolution of the Karoo Graben of northern Malawi (East Africa). *Geologische Rundschau*, *84*(3), 607–625. https://doi.org/10.1007/bf00284524

Roberts, E. M., O'Connor, P. M., Stevens, N. J., Gottfried, M. D., Jinnah, Z. A., Ngasala, S., et al. (2010). Sedimentology and depositional environments of the red Sandstone group, Rukwa Rift basin, southwestern Tanzania: New insight into cretaceous and paleogene terrestrial ecosystems and tectonics in sub-equatorial Africa. *Journal of African Earth Sciences*, *57*(3), 179–212. https://doi.org/10.1016/j.jafrearsci.2009.09.002

Roberts, E. M., Stevens, N., O'Connor, P. M., Dirks, P., Gottfried, M. D., Clyde, W., et al. (2012). Initiation of the western branch of the East African Rift coeval with the eastern branch. *Nature Geoscience*, *5*(4), 289–294. https://doi.org/10.1038/ngeo1432

Rumvegeri, B. T. (1991). Tectonic significance of Kibaran structures in central and eastern Africa. *Journal of African Earth Sciences*, *13*(2), 267–276. https://doi.org/10.1016/0899-5362(91)90010-V

Ryan, W. B. F., Carbotte, S. M., Coplan, J., O'Hara, S., Melkonian, A., Arko, R., et al. (2009). Global Multi-Resolution Topography (GMRT) synthesis data set. *Geochemistry, Geophysics, Geosystems*, *10*(3), Q03014. https://doi.org/10.1029/2008GC002332

Samsu, A., Micklethwaite, S., Williams, J. N., Fagereng, Å., & Cruden, A. R. (2023). Structural inheritance in amagmatic rift basins: Manifestations and mechanisms for how pre-existing structures influence rift-related faults. *Earth-Science Reviews*, *246*, 104568. https://doi.org/10.1016/j.earscirev.2023.104568

Saria, E., Calais, E., Stamps, D. S., Delvaux, D., & Hartnady, C. J. H. (2014). Present-day kinematics of the East African rift. *Journal of Geophysical Research: Solid Earth*, *119*(4), 3584–3600. https://doi.org/10.1002/2013JB010901

Servais, T., & Sintubin, M. (2009). Avalonia, Armorica, Perunica: Terranes, microcontinents, microplates or palaeobiogeographical provinces? *Geological Society, London, Special Publications*, *325*(1), 103–115. https://doi.org/10.1144/sp325.5

Spyropoulos, C., Griffith, W. J., Scholz, C. H., & Shaw, B. E. (1999). Experimental evidence for different strain regimes of crack populations in a clay model. *Geophysical Research Letters*, *26*(8), 1081–1084. https://doi.org/10.1029/1999GL900175

Spyropoulos, C., Scholz, C. H., & Shaw, B. E. (2002). Transition regimes for growing crack populations. *Physical Review E*, *65*(5), 056105. https://doi.org/10.1103/PhysRevE.65.056105

Stern, J. R. (1994). Neoproterozoic (900–550 Ma) arc assembly and continental collision in the East Africa Orogen: Implications for the consolidation of Gondwanaland. *Annual Review of Earth and Planetary Sciences*, *22*(1), 319–351. https://doi.org/10.1146/annurev.ea.22.050194.001535

Tack, L., Liégeois, J. P., Deblond, A., & Duchesne, J. C. (1994). Kibaran A-type Granitoids and mafic rocks generated by two mantle sources in a late orogenic setting (Burundi). *Precambrian Research*, *68*(3), 323–356. https://doi.org/10.1016/0301-9268(94)90036-1

Tack, L., Wingate, M. T. D., De Waele, B., Meert, J., Belousova, E., Griffin, B., et al. (2010). The 1375 Ma "Kibaran event" in Central Africa: Prominent emplacement of bimodal magmatism under extensional regime. *Precambrian Research*, *180*(1), 63–84. https://doi.org/10.1016/j.precamres.2010.02.022

Theunissen, K., Klerkx, J., Melnikov, A., & Mruma, A. (1996). Mechanisms of inheritance of rift faulting in the western branch of the East African Rift, Tanzania. *Tectonics*, *15*(4), 776–790. https://doi.org/10.1029/95TC03685

Theunissen, K., Lenoir, J., Liegeois, J., Delvaux, D., & Mruma, A. (1992). Major Pan-African Imprint in the Ubendian belt of SW Tanzania-U–PB on zircon geochronology and structural context. *Comptes Rendus de l Academie des Sciences Serie II*, *314*(12), 1355–1362.

Thiéblemont, D., Callec, Y., Fernandez-Alonso, M., & Chène, F. (2018). A geological and isotopic framework of Precambrian terrains in western central Africa: An introduction. *Geology of Southwest Gondwana*, 107–132. https://doi.org/10.1007/978-3-319-68920-3_5

Tshibangu, J.-P., & Descamps, F. (2016). Redesigning the geometry of the Makala Coal Mine to improve safety and productivity. In *3rd international symposium on mine safety science and engineering, 197(2016)*

Uieda, L., Tian, D., Leong, W. J., Toney, L., Schlitzer, W., Grund, M., et al. (2021). PyGMT: A Python interface for the generic mapping Tools. *Zenodo*. https://doi.org/10.5281/ZENODO.4522136

van Herwaarden, D.-P., Thrastarson, S., Hapla, V., Afanasiev, M., Trampert, J., & Fichtner, A. (2023). Full-waveform tomography of the African Plate using dynamic mini-batches. *Journal of Geophysical Research: Solid Earth*, *128*(6), e2022JB026023. https://doi.org/10.1029/2022jb026023

Veatch, A. C., & Geological Society of America. (1935). Evolution of the Congo basin. [New York]: The society.

Versfelt, J., & Rosendahl, B. R. (1989). Relationships between pre-rift structure and rift architecture in lakes Tanganyika and Malawi, East Africa. *Nature*, *337*(6205), 354–357. https://doi.org/10.1038/337354a0

Villeneuve, M. (1977). *Précambrien du Sud du lac Kivu (région du Kivu, République du Zaïre). Etude stratigraphique, pétrographique et tectonique*. (PhD Thesis). Université d'Aix-Marseille Ill.

Villeneuve, M. (1987). Géologie du synclinal de l'Itombwe (Zaïre oriental) et le problème de l'existence d'un sillon plissé pan-Africain. *Journal of African Earth Sciences*, *6*(6), 869–880. https://doi.org/10.1016/0899-5362(87)90046-7

Vink, G. E., Morgan, W. J., & Zhao, W.-L. (1984). Preferential rifting of continents: A source of displaced terranes. *Journal of Geophysical Research*, *89*(B12), 10072–10076. https://doi.org/10.1029/JB089iB12p10072

Wakenge, C. I., & Matthysen, K. (2023). Securing insecurity: Semi-industrial gold mining and violence in Mwenga, south Kivu, democratic republic of Congo. *IPIS, Bukavu/Antwerp*. https://ipisresearch.be/publication/semi-industrial-gold-mining-and-violence-in-mwenga-south-kivu-democratic-republic-of-congo/

Walemba, K. M. A. (2001). Geology, geochemistry, and tectono-metallogenic evolution of neuproterozoic gold deposits in the Kadubu area, Kivu, Democratic Republic of Congo. Retrieved from http://hdl.handle.net/10539/15209

Wauthier, C., Smets, B., & Keir, D. (2015). Diking-induced moderate-magnitude earthquakes on a youthful rift border fault: The 2002 Nyiragongo-Kalehe sequence, D. R. Congo. *Geochemistry, Geophysics, Geosystems*, *16*(12), 4280–4291. https://doi.org/10.1002/2015gc006110

Wedmore, L. N. J., Evans, D., Williams, J. N., Biggs, J., Fagereng, A., Mawejje, P., et al. (2024). The early onset of magmatic rift faulting in the Edward-George Rift, Uganda. *Earth and Planetary Science Letters*, *638*, 118762. https://doi.org/10.1016/j.epsl.2024.118762

Wedmore, L. N. J., Williams, J. N., Biggs, J., Fagereng, Å., Mphepo, F., Dulanya, Z., et al. (2020). Structural inheritance and border fault reactivation during active early-stage rifting along the Thyolo fault, Malawi. *Journal of Structural Geology*, *139*, 104097. https://doi.org/10.1016/j.jsg.2020.104097

Wessel, P., Luis, J. F., Uieda, L., Scharroo, R., Wobbe, F., Smith, W. H. F., & Tian, D. (2019). The generic mapping Tools version 6. *Geocheistry, Geophysics, Geosystems*, *20*(11), 5556–5564. https://doi.org/10.1029/2019gc008515

Williams, J. N., Fagereng, Å., Wedmore, L. N. J., Biggs, J., Mphepo, F., Dulanya, Z., et al. (2019). How do variably striking faults reactivate during rifting? Insights from southern Malawi. *Geochemistry, Geophysics, Geosystems*, *20*(7), 3588–3607. https://doi.org/10.1029/2019GC008219

Williams, J. N., Wedmore, L. N. J., Scholz, C. A., Kolawole, F., Wright, L. J. M., Shillington, D. J., et al. (2022). The Malawi active fault database: An onshore-offshore database for regional assessment of seismic hazard and tectonic evolution. *Geochemistry, Geophysics, Geosystems*, *23*(5), e2022GC010425. https://doi.org/10.1029/2022GC010425

Withjack, M. O., Schlische, R. W., Olsen, P. E., Roberts, D., & Bally, A. (2012). Development of the passive margin of eastern North America: Mesozoic rifting, igneous activity, and breakup. *Regional Geology and Tectonics: Phanerozoic Rift Systems and Sedimentary Basins*, *1*, 301.

References From the Supporting Information

Dziewonski, A. M., Chou, T.-A., & Woodhouse, J. H. (1981). Determination of earthquake source parameters from waveform data for studies of global and regional seismicity. *Journal of Geophysical Research*, *86*(B4), 2825–2852. https://doi.org/10.1029/JB086iB04p02825

Fishwick, S. (2010). Surface wave tomography: Imaging of the lithosphere-aesthenosphere boundary beneath central and Southern Africa? *Lithos*, *120*(1–2), 63–73. https://doi.org/10.1016/j.lithos.2010.05.011

Pasyanos, M. E., Masters, G., Laske, G., & Ma, Z. (2014). LITHO1.0: An updated crust and lithospheric model of the Earth. *JGR Solid Earth*, *119*(3), 2153–2173. https://doi.org/10.1002/2013jb010626